

Quark–Gluon Vertex from Lattice QCD

Jonivar Skullerud

*Instituut voor Theoretische Fysica, Universiteit van Amsterdam, Valckenierstraat 65,
NL-1018 XE Amsterdam, The Netherlands*

Ayşe Kızılersü

*Special Research Centre for the Subatomic Structure of Matter, University of Adelaide,
Adelaide SA 5005, Australia*

ABSTRACT: The quark–gluon vertex in Landau gauge is studied in the quenched approximation using the Sheikholeslami–Wohlert (SW) fermion action with mean-field improvement coefficients in the action and for the quark fields. We see that the form factor that includes the running coupling is substantially enhanced in the infrared, over and above the enhancement arising from the infrared suppression of the quark propagator alone. We define two different momentum subtraction renormalisation schemes — $\overline{\text{MOM}}$ (asymmetric) and $\overline{\text{MOM}}$ (symmetric) — and determine the running coupling in both schemes. We find $\Lambda_{\overline{\text{MS}}}^{N_f=0} = 300_{-180}^{+150} \pm 55 \pm 30$ MeV from the asymmetric scheme. This is somewhat higher than other determinations of this quantity, but the uncertainties — both statistical and systematic — are large. In the symmetric scheme, statistical noise prevents us from obtaining a meaningful estimate for $\Lambda_{\overline{\text{MS}}}$.

KEYWORDS: Renormalization Regularization and Renormalons, Nonperturbative Effects, QCD, Lattice QCD.

Contents

1. Introduction	1
2. Definitions and principles	4
3. Definition of the MOM schemes	7
4. Lattice formalism and computational details	8
5. Determination of Z_2 and Z_3	9
6. λ_1 and the running coupling	11
6.1 Asymmetric scheme	11
6.2 Symmetric scheme	17
7. Matching to $\overline{\text{MS}}$	17
8. Discussion and outlook	19
A. Tensor decomposition of the vertex	21
B. Tree-level lattice expressions	23
B.1 Asymmetric kinematics	25
B.2 Symmetric kinematics	25
C. One-loop expressions	27

1. Introduction

The quark–gluon vertex plays an important role in many applications of QCD. QCD vertex functions may be used to define momentum subtraction (MOM) renormalisation schemes [1, 2]. These, it is argued, are more ‘physical’ than the minimal subtraction (MS or $\overline{\text{MS}}$) schemes, since the latter can only be defined in a perturbative context, while the former are independent of the regularisation method and give a better guidance to the appropriate renormalisation scale for a particular problem. Recently, a complete determination of the quark–gluon vertex to one-loop order was performed [3]. In an asymmetric momentum subtraction scheme, it has recently been computed to three-loop order [4], while a numerical computation to two-loop order has been performed in a symmetric scheme [5].

The quark–gluon vertex from the lattice may thus yield a direct determination of the QCD running coupling α_s , to complement other methods for determining this quantity [6]. For a review of experimental and theoretical determinations of α_s , see [7].

In addition to reproducing the ultraviolet, perturbative behaviour, and thus determining the intrinsic QCD scale $\Lambda_{\overline{\text{MS}}}$, the quark–gluon vertex can also be used to probe the infrared behaviour of the running coupling. The hypothesis that the QCD coupling approaches a constant in the infrared has long been popular on phenomenological grounds, and has also received some theoretical support from ‘optimised’ perturbation theory [8]. On the other hand, a more recent proposal for reorganising perturbation theory [9] gives a running coupling that vanishes in the infrared. Lattice QCD may in principle assist in resolving this issue.

The nonperturbative quark–gluon vertex also enters into the Dyson–Schwinger equations (DSEs) [10, 11, 12], which are the QCD field equations. In particular, in Minkowski space the DSE for the renormalised quark propagator $S(p)$ is

$$S^{-1}(p) = Z_2(\not{p} - Z_m m) + i\frac{4}{3}Z_{1F}g^2 \int \frac{d^4k}{(2\pi)^4} \gamma_\mu S(k) D^{\mu\nu}(k-p) \Gamma_\nu(p, k-p), \quad (1.1)$$

where m and g are the renormalised mass and coupling respectively. The unknown quantities here are the nonperturbative gluon propagator $D_{\mu\nu}(q)$ and the quark–gluon vertex $\Gamma_\mu(p, q)$ [see figure 1]. Z_2 and Z_m are the quark field and mass renormalisation constants respectively. It will be convenient to also introduce $\Lambda_\nu(p, q) \equiv -ig\Gamma_\nu(p, q)$.

Since these are gauge dependent quantities, it is to be expected that the confinement picture, and the relative importance of the various factors, will vary between different gauges. We will here be working in the (minimal) Landau gauge, where over the past few years substantial progress has been made in our understanding of the gluon propagator from lattice simulations [13, 14, 15, 16] as well as analytical studies [17].

The quark self-energy directly exhibits confinement and dynamical chiral symmetry breaking, and is an important input for phenomenological models of hadron physics [10]. It has also recently been evaluated in Landau gauge on the lattice [18, 19, 20, 21].

However, the quark–gluon vertex remains largely unknown, and the validity of the usual ansätze untested. In Landau gauge, there are indications that it must contain non-trivial structure in the infrared. The lattice (infrared suppressed) gluon propagator together with a bare or QED-like vertex fails to yield solutions to (1.1) that exhibit an appropriate degree of dynamical chiral symmetry breaking [22]. But there are also strong indications that the ghost propagator in Landau gauge is strongly enhanced, both from lattice simulations [23, 24] and analytical studies [17]. The ghost self-energy enters into the quark–gluon

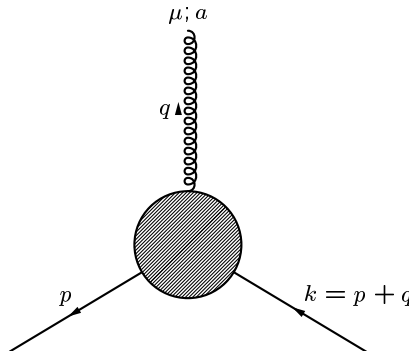


Figure 1: The quark–gluon vertex.

vertex through the Slavnov–Taylor identity,

$$q^\mu \Gamma_\mu(p, q) = G(q^2) [(1 - B(q, p + q))S^{-1}(p) - S^{-1}(p + q)(1 - B(q, p + q))] , \quad (1.2)$$

where $G(q^2)$ is the ghost renormalisation function and $B^a(q, k) = t^a B(q, k)$ is the ghost–quark scattering kernel, which is given by the diagram in figure 2. It appears that modelling this into the quark DSE does give solutions exhibiting chiral symmetry breaking and quark confinement [25].

A nonperturbative determination of the quark–gluon vertex will therefore give us further insight into the mechanisms of confinement and chiral symmetry breaking, as well as casting light on the transition between the perturbative and nonperturbative regimes of QCD.

The starting point for analytical studies of the quark–gluon vertex is the QED vertex, which gives the ‘abelian’ contribution to the QCD vertex. In the abelian case, the Slavnov–Taylor identity implies that the vertex can be written entirely as a function of the nonperturbative quark propagator up to a transverse term, as shown by Ball and Chiu [26]. A kinematical basis, along with a one-loop determination of all the components, is given in [26, 27].

The three-gluon vertex has been the subject of detailed study in recent years [28, 29].

An important result of these studies is the discovery of substantial power corrections to the running coupling, which remain up to scales of 7–10 GeV, and originate from the $\langle AA \rangle$ condensate appearing in the Landau gauge OPE. It has been conjectured that this condensate is largely due to instanton effects [30]. In the quark–gluon vertex the situation is in some senses more straightforward. Power corrections due to the quark mass appear already in the one-loop perturbative running coupling, and these are expected to be substantially enhanced by the chiral condensate. These are phenomena that will appear in any gauge. Any correction due to a covariant-gauge $\langle AA \rangle$ condensate will come in addition to this.

This paper builds on earlier results that were presented in [31]. We will be focusing on the form factor multiplying γ_μ , which contains the running coupling. We investigate the infrared behaviour of this form factor, to study the hypothesis of infrared enhancement, as well as the ultraviolet behaviour, attempting to determine the perturbative running.

In section 2 we define our notation and the quantities involved. In section 3 we define two momentum subtraction schemes based on the quark–gluon vertex, which we call $\overline{\text{MOM}}$ and $\overline{\text{MOM}}$, and explain how the running coupling may be extracted in these schemes. The parameters of our simulations are given in section 4. In section 5 we determine the quark and gluon field renormalisation constants Z_2 and Z_3 . Our results for the λ_1 form factor and the $\overline{\text{MOM}}$ running coupling are given in section 6.1, while the results for the $\overline{\text{MOM}}$ scheme are given in section 6.2. In section 7 we translate the $\overline{\text{MOM}}$ scheme results to the $\overline{\text{MS}}$

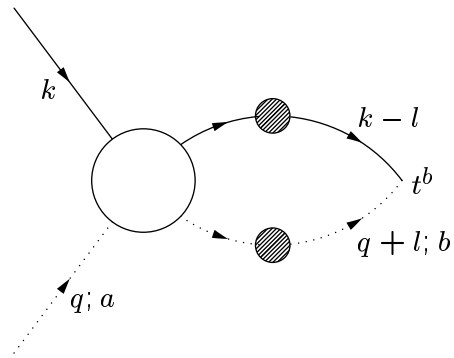


Figure 2: The ghost-quark scattering kernel B^a .

scheme. Finally, in section 8 we summarise our conclusions and discuss the prospects for further work. The appendices contain a discussion of the full tensor decomposition of the vertex; the lattice tree-level expressions and our method for removing the dominant (tree-level) lattice artefacts; and the full one-loop continuum expressions for the form factors we consider.

2. Definitions and principles

With the exception of section 7, where the perturbative expressions are given in Minkowski space, we will be working throughout in euclidean space, with a positive metric, such that $A^2 > 0$ for any spacelike vector A . The commutation relations for the Dirac matrices are the usual ones,

$$\{\gamma_\mu, \gamma_\nu\} = 2\delta_{\mu\nu}; \quad \gamma_\mu^\dagger = \gamma_\mu. \quad (2.1)$$

The $\sigma_{\mu\nu}$ -matrices are defined by

$$\sigma_{\mu\nu} \equiv \frac{1}{2}[\gamma_\mu, \gamma_\nu]. \quad (2.2)$$

The generators t^a of the Lie algebra have the conventional normalisation, $\text{Tr}(t^a t^b) = \frac{1}{2}\delta^{ab}$.

We can define the configuration space quark–gluon vertex function (see figure 1) on the lattice as

$$V_\mu^a(x, y, z)_{\alpha\beta}^{ij} = \left\langle \psi_\alpha^i(x) \bar{\psi}_\beta^j(z) A_\mu^a(y) \right\rangle = \left\langle \left\langle S_{\alpha\beta}^{ij}(x, z) A_\mu^a(y) \right\rangle \right\rangle. \quad (2.3)$$

Here, $\langle \dots \rangle$ denotes averaging over all fermion and gauge field configurations, while $\langle\langle \dots \rangle\rangle$ denotes averaging over gauge field configurations only. Fourier transforming this and invoking translational invariance gives us the full (unamputated) momentum space bare vertex function $V_\mu^a(p, q)$:

$$\begin{aligned} & \sum_{x,y,z} e^{-i(p \cdot x + q \cdot y - k \cdot z)} \left\langle \psi_\alpha^i(x) A_\mu^a(y) \bar{\psi}_\beta^j(z) \right\rangle \\ &= \sum_z e^{-i(p-k+q) \cdot z} \sum_{x,y} e^{-i(p \cdot x + q \cdot y)} \left\langle \psi_\alpha^i(x) A_\mu^a(y) \bar{\psi}_\beta^j(0) \right\rangle \\ &= V \delta(p-k+q) \left\langle \left\langle S_{\alpha\beta}^{ij}(p; U) A_\mu^a(q) \right\rangle \right\rangle \equiv V \delta(p-k+q) V_\mu^a(p, q)_{\alpha\beta}^{ij}, \quad (2.4) \end{aligned}$$

where V is the lattice volume. The proper (one-particle irreducible) bare vertex Λ_μ can be obtained by amputating the external quark and gluon legs from the full vertex V_μ^a :

$$\Lambda_\mu^{a,\text{lat}}(p, q) = S(p)^{-1} V_\mu^a(p, q) S(p+q)^{-1} D(q)_{\nu\mu}^{-1}. \quad (2.5)$$

The only possible dependence this can have on the group coordinates a, i, j is proportional to the generator t_{ij}^a . We can therefore consider only $\Lambda_\mu(p, q)$, defined by

$$(\Lambda_\mu^a)_{\alpha\beta}^{ij} = t_{ij}^a (\Lambda_\mu)_{\alpha\beta} \equiv -ig_0 t_{ij}^a (\Gamma_\mu)_{\alpha\beta}. \quad (2.6)$$

$S(p) = \langle\langle S(p; U) \rangle\rangle = \langle\langle \sum_x e^{-ipx} S(x, 0; U) \rangle\rangle$ is the momentum-space quark propagator, while $D(q)$ is the gluon propagator, which in the infinite-volume limit takes the form

$$D_{\mu\nu}^{ab}(q) = \delta^{ab} D_{\mu\nu}(q) = \delta^{ab} \left(\delta_{\mu\nu} - \frac{q_\mu q_\nu}{q^2} \right) D(q^2) + \delta^{ab} \xi \frac{q_\mu q_\nu}{q^2} \frac{1}{q^2}. \quad (2.7)$$

In the Landau gauge ($\xi=0$), $D(q^2)$ can be determined for $q \neq 0$ by

$$D(q^2) = \frac{1}{3(N_C^2 - 1)} \sum_{\mu, a} D_{\mu\mu}^{aa}(q). \quad (2.8)$$

As long as q is not too close to zero, this form remains valid also for a finite volume. In general, a finite volume will induce an effective ‘mass’ $m \sim 1/L$, which on an asymmetric lattice may also be direction-dependent — so the tensor structure (2.7) must be replaced by [13]

$$D_{\mu\nu}^{ab}(q) = \delta^{ab} \left(\delta_{\mu\nu} - \frac{h_{\mu\nu}(q)}{f(q^2)} \right) D(q^2) + \delta^{ab} \xi \frac{h'_{\mu\nu}}{g(q^2)} \equiv \delta^{ab} T_{\mu\nu}(q) D(q) + \delta^{ab} \xi \frac{h'_{\mu\nu}(q)}{g(q^2)}, \quad (2.9)$$

where the functions f, g, h, h' are such that for sufficiently large q , (2.9) approaches the infinite-volume form, but both f and g remain non-zero as $q \rightarrow 0$. The Landau-gauge expression (2.8) must for the smallest momentum values — and in particular for $q = 0$ on any volume — be replaced by

$$D(q^2) = \frac{1}{(N_C^2 - 1)} \sum_{\mu, a} D_{\mu\mu}^{aa}(q) / \sum_{\mu} T_{\mu\mu}(q) \equiv \frac{1}{T(q)(N_C^2 - 1)} \sum_{\mu, a} D_{\mu\mu}^{aa}(q). \quad (2.10)$$

In the infinite-volume limit, $T_{\mu\nu}(0) \rightarrow \delta_{\mu\nu}$ since the Landau gauge condition places no restriction on the zero-modes [32], so $T(0) \rightarrow 4$. In [13] it was found that an asymmetric finite volume may induce large distortions to this form, and in general the components must be determined numerically. However, $T_{\mu\nu}(0)$ will always remain diagonal.

Since the gluon propagator in Landau gauge for $q \neq 0$ becomes proportional to the transverse projector $P_{\mu\nu}(q) \equiv \delta_{\mu\nu} - q_\mu q_\nu / q^2$ or its lattice equivalent, D^{-1} is undefined and we cannot use eq. (2.5). Instead, we rewrite (2.5) as follows,

$$D_{\mu\nu}(q) \Lambda_\nu^a(p, q) = P_{\mu\nu}(q) D(q^2) \Lambda_\nu^a(p, q) = S(p)^{-1} V_\mu^a(p, q) S(p+q)^{-1}, \quad (2.11)$$

from which we can obtain the transverse-projected vertex,

$$\Lambda_\mu^{a,P}(p, q) \equiv P_{\mu\nu}(q) \Lambda_\nu^{a,\text{lat}}(p, q) = S(p)^{-1} V_\mu^a(p, q) S(p+q)^{-1} D(q^2)^{-1}. \quad (2.12)$$

The quantities calculated on the lattice are always functions of the bare (unrenormalised) fields ψ^0, A_μ^0 and the bare coupling g_0 . The relation between renormalised and bare quantities is given by

$$\psi^0 = Z_2^{1/2} \psi; \quad \bar{\psi}^0 = Z_2^{1/2} \bar{\psi}; \quad A_\mu^0 = Z_3^{1/2} A_\mu; \quad g_0 = Z_g g; \quad \xi_0 = Z_3 \xi, \quad (2.13)$$

where Z_2, Z_3, Z_g are the quark, gluon and vertex (coupling) renormalisation constants respectively, and are functions of the regularisation parameter a and the renormalisation scale μ . From (2.13) it follows that

$$S^{\text{bare}}(p; a) = Z_2(\mu; a)S(p; \mu); \quad (2.14)$$

$$D^{\text{bare}}(q^2; a) = Z_3(\mu; a)D(q^2; \mu). \quad (2.15)$$

The renormalised vertex is related to the bare vertex according to

$$\Lambda_\mu^{\text{bare}}(p, q; a) = Z_{1F}^{-1}(\mu; a)\Lambda_\mu(p, q; \mu). \quad (2.16)$$

Gauge invariance requires that $Z_{1F} = Z_g Z_2 Z_3^{1/2}$, and so we may write

$$\Lambda_\mu^{\text{bare}}(p, q; a) = Z_g^{-1}(\mu; a)Z_2^{-1}(\mu; a)Z_3^{-1/2}(\mu; a)\Lambda_\mu(p, q; \mu), \quad (2.17)$$

meaning that only the quark and gluon fields, along with the running coupling, are independently renormalised. For the sake of brevity, we will from here on no longer explicitly label bare quantities as such. Z_2 and Z_3 may be determined by imposing momentum subtraction (MOM) renormalisation conditions on the quark and gluon propagator respectively, demanding that they take on their tree-level forms at the renormalisation scale μ :

$$S(p; \mu) \Big|_{p^2=\mu^2} = \frac{1}{i \not{p} + m(\mu)}; \quad (2.18)$$

$$D(q^2; \mu) \Big|_{q^2=\mu^2} = \frac{1}{\mu^2}. \quad (2.19)$$

The renormalisation of the coupling will be discussed in section 3.

The Lorentz structure of the vertex in the continuum consists of 12 independent vectors and can be written in terms of a ‘Slavnov–Taylor’ (non-transverse) and purely transverse part in terms of vectors L_i, T_i and scalar functions λ_i, τ_i :

$$\begin{aligned} \Lambda_\mu(p, q) &= \Lambda_\mu^{(ST)}(p, q) + \Lambda_\mu^{(T)}(p, q) \\ &= -ig \sum_{i=1}^4 \lambda_i(p^2, q^2, k^2) L_{i,\mu}(p, q) - ig \sum_{i=1}^8 \tau_i(p^2, q^2, k^2) T_{i,\mu}(p, q). \end{aligned} \quad (2.20)$$

The full expressions for all the vectors L_i and T_i are given in appendix A. In this paper, we will only study the part of the vertex proportional to γ_μ , which in the specific kinematics we will be employing is given by the three vectors

$$L_{1,\mu} = \gamma_\mu; \quad L_{2,\mu} = -(2 \not{p} + \not{q})(2p + q)_\mu; \quad T_{3,\mu} = \not{q}q_\mu - q^2 \gamma_\mu. \quad (2.21)$$

Because of the Slavnov–Taylor identity (1.2), the scalar functions $\lambda_i(p^2, q^2, k^2)$ in (2.20) may be expressed in terms of the quark propagator, ghost propagator and ghost–quark scattering kernel. In QED for instance, as a result of the Ward–Takahashi identity, λ_1 is given uniquely in terms of the fermion propagator $S^{-1}(p) = i \not{p}A(p^2) + B(p^2)^1$ by [26]

$$\lambda_1^{\text{QED}}(p^2, q^2, k^2) = \frac{1}{2} (A(p^2) + A(k^2)). \quad (2.22)$$

¹Note that the opposite conventions for the B -function are often used in Minkowski space: our B corresponds to $-\beta$ in [3, 26]

In QCD, for $q = 0$, the equivalent of this is [33]

$$\lambda_1(p^2, 0, p^2) = G(0) \left[A(p^2) \chi_0(p^2, 0, p^2) + B(p^2) (\chi_1(p^2, 0, p^2) + \chi_2(p^2, 0, p^2)) - 2p^2 A(p^2) \chi_3(p^2, 0, p^2) \right], \quad (2.23)$$

where χ_i are the form factors of the ghost-quark scattering kernel given in [3]. At tree level, $\chi_0 = 1, \chi_{1,2,3} = 0$.

As already mentioned, in Landau gauge, for $q^2 \neq 0$, we can only determine the transverse part of the vertex from the lattice. The transverse projection of L_1 is

$$P_{\mu\nu}(q) L_{1,\nu}(p, q) = -\frac{1}{q^2} T_{3,\mu}(p, q). \quad (2.24)$$

This gives rise to the modified form factor λ'_1 ,

$$\lambda'_1 = \lambda_1 - q^2 \tau_3, \quad (2.25)$$

which will be useful when studying the transverse-projected vertex.

3. Definition of the MOM schemes

We impose the momentum subtraction scheme

$$\lambda_1(\mu) = 1, \quad (3.1)$$

where ‘ $\lambda_1(\mu)$ ’ stands for λ_1 evaluated at a specific kinematic point (e.g., symmetric or zero-momentum), with the momentum scale μ . The precise meaning of this will be clear when we discuss the $\widetilde{\text{MOM}}$ and $\overline{\text{MOM}}$ schemes. It then follows from (2.17) that

$$\begin{aligned} g_R(\mu) &= Z_g^{-1}(\mu; a) g_0(a) = Z_2(\mu; a) Z_3^{1/2}(\mu; a) g_0(a) \frac{\lambda_1^{\text{bare}}(\mu; a)}{\lambda_1(\mu)} \\ &= Z_2(\mu; a) Z_3^{1/2}(\mu; a) g_0(a) \lambda_1^{\text{bare}}(\mu; a). \end{aligned} \quad (3.2)$$

$g_0 \lambda_1^{\text{bare}}$ is the quantity we calculate on the lattice.

We will define two different renormalisation schemes, $\widetilde{\text{MOM}}$ and $\overline{\text{MOM}}$. The ‘asymmetric’ $\widetilde{\text{MOM}}$ scheme is defined by setting the gluon momentum q^2 to zero. This differs from the $\overline{\text{MOM}}$ scheme defined in [2], and also from the $\widetilde{\text{MOM}}_q$ scheme defined and computed to three-loop order in [4], where in both cases one of the quark momenta has been set to zero. The ‘symmetric’ $\overline{\text{MOM}}$ scheme is defined by the kinematics $p = -k = -q/2 = s$, so $p^2 = k^2 = q^2/4 = s^2$. The fully symmetric scheme where $p^2 = q^2 = k^2$ is impossible to implement on a finite lattice where the boundary conditions are different for fermions and gauge fields (antiperiodic and periodic in time respectively), which is why we are not considering it here.

In any scheme, the first step towards extracting the running coupling, which is proportional to λ_1 , is to eliminate those form factors with a different Dirac structure by tracing the vertex with γ_μ . With this in mind, we define the functions $H_\mu(p, q)$ as

$$\begin{aligned} H_\mu(p, q) &\equiv -\frac{1}{4} \text{Im Tr } \gamma_\mu \Lambda_\mu(p, q) \\ &= g_0 \left\{ \lambda_1 - (2p + q)_\mu^2 \lambda_2 + [(p \cdot q) q_\mu - q^2 p_\mu] (2p + q)_\mu \tau_2 \right. \\ &\quad \left. - (q^2 - q_\mu^2) \tau_3 - [q \cdot (2p + q) - q_\mu (2p + q)_\mu] \tau_6 \right\}, \end{aligned} \quad (3.3)$$

where no sum over μ is implied.

In the $\widetilde{\text{MOM}}$ scheme, all terms in (3.3) proportional to q or q_μ disappear, and we are left with

$$H_\mu(p, q = 0) = g_0 \left(\lambda_1(p^2, 0, p^2) - 4p_\mu^2 \lambda_2(p^2, 0, p^2) \right). \quad (3.4)$$

We can then eliminate λ_2 by imposing an appropriate kinematics: $p_\mu = 0, p_\nu \neq 0$ for $\mu \neq \nu$. This defines $\lambda_1^{\widetilde{\text{MOM}}}(\mu) \equiv \lambda_1(\mu^2, 0, \mu^2)$.

The $\widetilde{\text{MOM}}$ renormalised coupling is then defined as

$$g_{\widetilde{\text{MOM}}}(\mu) = Z_2(\mu) Z_3^{1/2}(\mu) g_0 \lambda_1^{\widetilde{\text{MOM}}}(\mu^2, 0, \mu^2). \quad (3.5)$$

In the $\overline{\text{MOM}}$ scheme, the transverse-projected vertex gives us

$$\begin{aligned} H_\mu^T(p, -2p) &= g_0 (4p^2 - 4p_\mu^2) \left(\frac{1}{4p^2} \lambda_1(p^2, 4p^2, p^2) - \tau_3(p^2, 4p^2, p^2) \right) \\ &\equiv g_0 \left(1 - \frac{p_\mu^2}{p^2} \right) \lambda_1'(p^2, 4p^2, p^2). \end{aligned} \quad (3.6)$$

λ_1' can then easily be extracted by

$$\lambda_1'(p^2, 4p^2, p^2) = \frac{1}{3} \sum_\mu H_\mu(p, -2p) \equiv \frac{1}{3} h_1(p^2). \quad (3.7)$$

Thus, we define the $\overline{\text{MOM}}$ running coupling as

$$g_{\overline{\text{MOM}}}(\mu) = Z_2(\mu) Z_3^{1/2}(\mu) g_0 \lambda_1'(\mu^2, 4\mu^2, \mu^2). \quad (3.8)$$

4. Lattice formalism and computational details

In this study, we use the Sheikholeslami–Wohlert fermion action,

$$S_{SW} = S_W - i \frac{a}{4} g_0 c_{sw} \sum_x \sum_{\mu\nu} \bar{\psi}(x) \sigma_{\mu\nu} F_{\mu\nu}(x) \psi(x), \quad (4.1)$$

which is on-shell $\mathcal{O}(a)$ -improved (S_W is the Wilson action), along with an off-shell improved² quark propagator S_I , given by [18]

$$S_I(x, y) = (1 + b_q m a) S_0(x, y) - 2a c_q' \delta(x - y), \quad (4.2)$$

²For full off-shell improvement, there should also be a gauge dependent improvement term. The absence of this term will give rise to errors, potentially of $\mathcal{O}(g^2 a)$ [34]. We assume that this is a small effect compared with other systematic errors. Setting this term to zero is also consistent with mean-field improvement, which is what we are using in this paper.

where the ‘unimproved’ quark propagator S_0 is simply derived from the inverse of the fermion matrix M : $S_0(x, y) = \langle M^{-1}(x, y; U) \rangle$.

We define the lattice gluon field A_μ , which in the continuum limit becomes aA_μ^{cont} , as

$$\begin{aligned} A_\mu(q) &\equiv \sum_x e^{-iq \cdot (x + \hat{\mu}/2)} A_\mu(x + \hat{\mu}/2) \\ &= \frac{e^{-iq_\mu a/2}}{2ig_0} \left[\left(U_\mu(q) - U_\mu^\dagger(-q) \right) - \frac{1}{3} \text{Tr} \left(U_\mu(q) - U_\mu^\dagger(-q) \right) \right]. \end{aligned} \quad (4.3)$$

In order to reduce lattice artefacts, we employ a tree-level correction scheme, as discussed at length in [18, 19]. The relevant tree-level expressions, and the definition of the tree-level corrected vertex form factors, are given in appendix B.

All the results in this paper have been obtained with the Wilson gauge action at $\beta = 6.0$ on a $16^3 \times 48$ lattice. Using the hadronic radius r_0 [35, 36] to set the scale, this corresponds to a lattice spacing $a^{-1} = 2.12$ GeV. The gauge fields were generated with a Hybrid Over-Relaxed algorithm, with configurations separated by 800 sweeps. The quark propagators have been generated using a mean-field improved SW fermion action, with $c_{\text{sw}} = 1.479$, for one value of $\kappa = 0.1370$, or $ma = 0.0579$. Details of the computation are given in [37]. For the improvement coefficients b_q and c'_q of (4.2) we have used the mean-field values $b_q = 1.14, 2c'_q = 0.57$.

The gauge fields have been fixed to Landau gauge, using a Fourier accelerated algorithm [38] to deal with low-momentum modes. The Landau gauge condition has been achieved to an accuracy of $\frac{1}{\sqrt{N_C}} \sum_{x,\mu} |\partial_\mu A_\mu|^2 < 10^{-12}$. Further details of the gauge fixing are given in [13].

For the quark fields, we have used periodic boundary conditions in the spatial directions and antiperiodic boundary conditions in the time direction. Hence, the available momentum values for an $N_i^3 \times N_t$ lattice (with N_i, N_t even numbers and $i = x, y, z$) are

$$p_i = \frac{2\pi}{N_i a} \left(n_i - \frac{N_i}{2} \right) \quad ; \quad n_i = 1, 2, \dots, N_i ; \quad (4.4)$$

$$p_t = \frac{2\pi}{N_t a} \left(n_t - \frac{1}{2} - \frac{N_t}{2} \right); \quad n_t = 1, 2, \dots, N_t . \quad (4.5)$$

For the gluon fields, we have used periodic boundary conditions in all directions, and thus we have integer momentum values also in the time direction. The gluon tensor structure was studied in [13]. Our data correspond to the ‘small lattice’ in that paper. There it was found that

$$T_{\mu\nu}(0) \sim \text{diag}(1, 1, 1, 1/3) \quad \implies \quad T(0) \approx \frac{10}{3}, \quad (4.6)$$

where $T_{\mu\nu}$ and T are defined in (2.9). Significant deviations from the infinite-volume form were also found for the lowest one or two momentum points used for the symmetric kinematics. We have explicitly adjusted these points to account for this. For all other momentum combinations we will be studying here, the deviation of $T_{\mu\nu}(q)$ from $P_{\mu\nu}^{\text{lat}}(q) = P_{\mu\nu}(Q(q))$ were found to be negligible.

5. Determination of Z_2 and Z_3

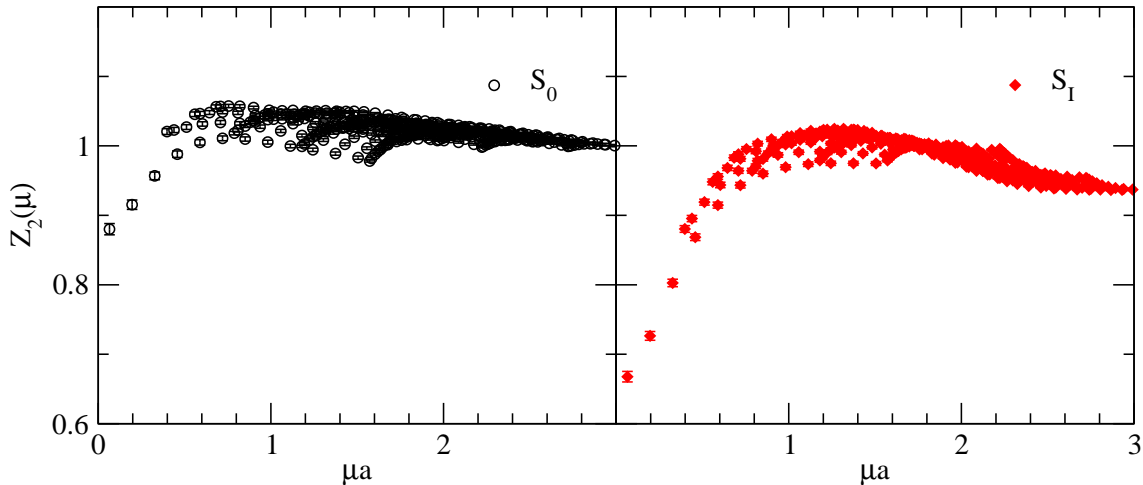


Figure 3: Z_2 as a function of the renormalisation scale μa , for S_0 (left) and for S_I (right), using the tree-level correction defined in (B.10), and without any momentum cuts .

In order to determine the quark field renormalisation constant Z_2 , we have used the tree-level corrected function $Z(p)$, defined in (B.10). The results, for both S_0 (for which $Z^{(0)}(p) \equiv 1$) and S_I are shown in figure 3.

In order to determine the gluon field renormalisation constant Z_3 , we use the simple tree-level correction procedure that was applied in [13]. The gluon propagator $D(q^2)$ is expressed in terms of the ‘lattice momentum’ Q [see (B.2)], and a ‘cylinder cut’ is applied to select momenta near the 4-diagonal. This is shown as a function of Qa in figure 4. We have fitted the gluon propagator to the phenomenological curve (Model A) of [13],

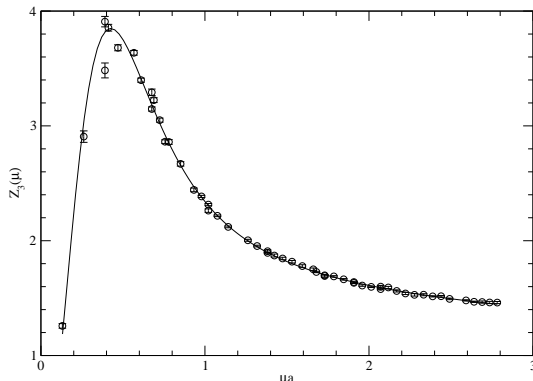


Figure 4: Z_3 as a function of the renormalisation scale μa , for 125 configurations. The line denotes the best fit to the functional form (5.1).

$$D(Q^2) = Z \left[\frac{AM^{2\alpha}}{(Q^2 + M^2)^{1+\alpha}} + \frac{1}{Q^2 + M^2} \left[\frac{1}{2} \ln((Q^2 + M^2)(Q^{-2} + M^{-2})) \right]^{-d_D} \right], \quad (5.1)$$

where $d_D = 13/22$ is the gluon anomalous dimension. The best estimates for the parameters are

$$Z = 2.02; \quad A = 10.7; \quad M = 0.534; \quad \alpha = 2.17. \quad (5.2)$$

It should be emphasised that this fit is only performed to facilitate the computation of the running coupling, and no physical significance should be attached to the phenomenological parameters quoted.

6. λ_1 and the running coupling

6.1 Asymmetric scheme

We have calculated the proper vertex in the asymmetric scheme using both the unimproved quark propagator S_0 and the improved propagator S_I .

We have evaluated λ_1 by first calculating $H_i(p, q = 0)$ ($i = 1, 2, 3$) for different values of p (with $p_i = 0$), and then used invariance under the (hyper-)cubic group to perform a Z_3 average over i and equivalent values of p_μ (as well as positive and negative p_μ values). But first, we want to verify that the cubic invariance really holds. As figure 5 shows, all the three spatial components of the (uncorrected) vertex do indeed behave in the same fashion, within errors. The discrepancies of the order 2σ can be put down to correlations between data at different momenta, combined with insufficient statistics.

When $p_\mu \neq 0$, $H_\mu(p, q)$ also receives a contribution from λ_2 . This means that we should not expect H_4 to behave similarly to the other three components, since $p_4 = p_t$ is necessarily non-zero. The lower panel of figure 5 confirms this — although part of the difference may also be due to finite volume effects affecting spatial and time directions differently. The form factor λ_2 will be studied in a forthcoming paper.

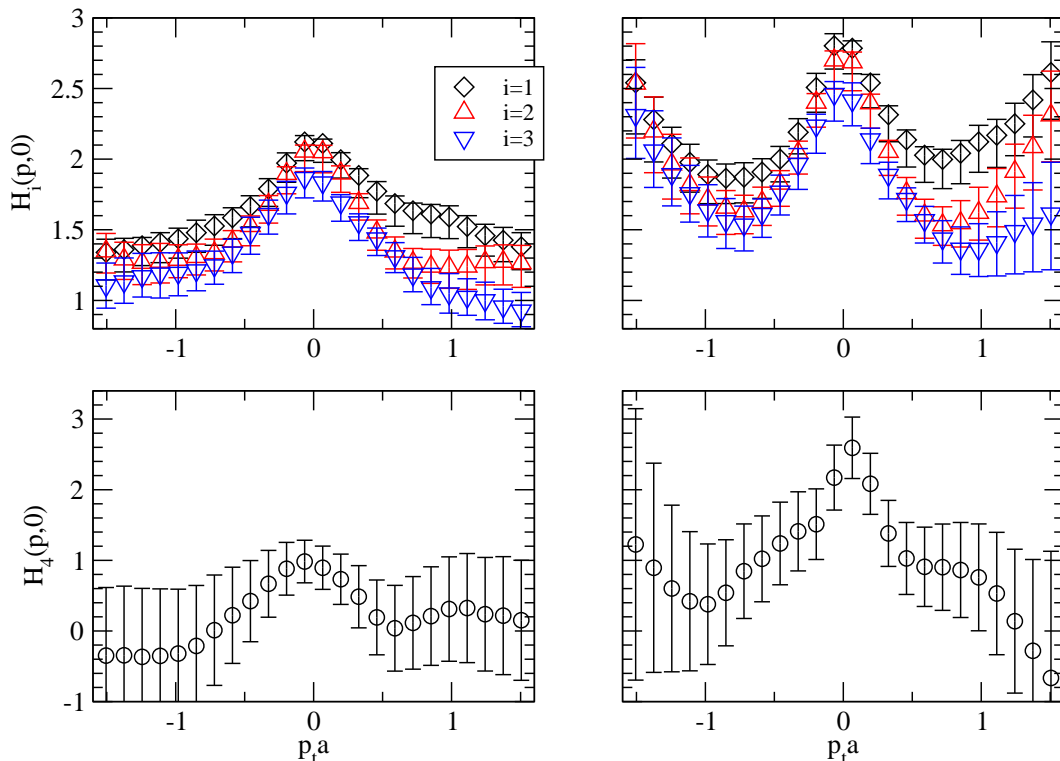


Figure 5: Top: $H_1(p, q)$, $H_2(p, q)$ and $H_3(p, q)$ for $q = 0$, $p = (0, p_t)$, as a function of $p_t a$; using S_0 (left) and S_I (right). Bottom: $H_4(p, q)$ for $q = 0$, $p = (0, p_t)$, as a function of $p_t a$, for 83 configurations using S_0 (left) and for 100 configurations using S_I (right). Note the different vertical scales for the upper and lower panels.

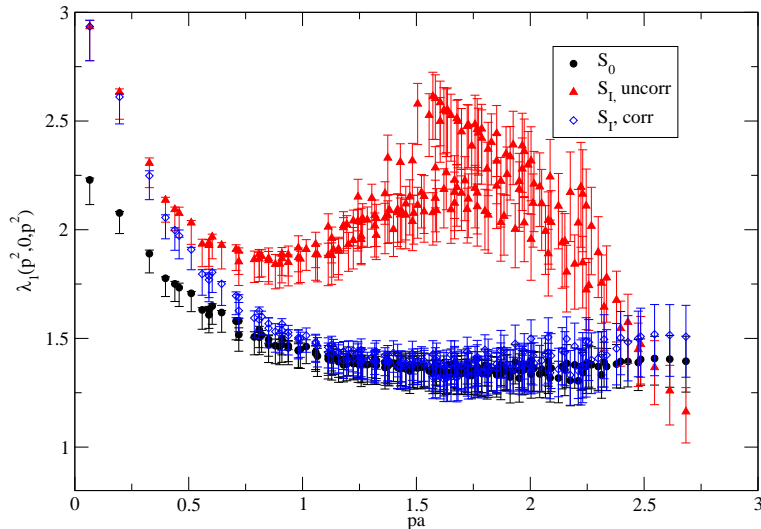


Figure 6: The unrenormalised form factor $\lambda_1(p^2, 0, p^2)$ as a function of $|pa|$, with equivalent momenta averaged. The form factor taken from the improved propagator S_I is shown both before and after tree-level correction. After tree-level correction, the lattice data for S_I lie on a single smooth curve.

In figure 6 we show the unrenormalised form factor λ_1 , obtained by averaging all $H_i(q = 0, p_i = 0)$ over equivalent momenta and directions, as a function of $|pa|$. As the figure shows, this is a well-defined function of p (within the statistical errors) for $pa \lesssim 1$, both when S_0 and S_I is used. For larger values of pa , however, λ_1 extracted using S_I develops significant ambiguities and a big ‘bump’ around $pa = 1.7$. This is due to the tree-level behaviour given in (B.15). Comparing with figure 1 of [18], we see that it is indeed approximately the inverse of the tree-level quark propagator. As expected, the irregular behaviour disappears after tree-level correction, and all the data lie on a single smooth curve. For $pa \gtrsim 1$ this curve coincides with the data for S_0 .

We clearly see a substantial infrared enhancement of λ_1 , in accordance with the expectations from studies of the gluon and ghost propagators. Part of this must be an ‘abelian’ enhancement given by the QED expression (2.22) together with the infrared suppression of the quark propagator. We can determine the additional, ‘non-abelian’ enhancement by plotting the product of λ_1 and the quark propagator form factor $Z(p)$, which in QED would be a momentum-independent constant. This is shown in figure 7, using the improved propagator S_I . As we can see, a significant enhancement over and above the ‘abelian’ one remains, although our lattice is too small to allow us to draw any further quantitative conclusions.

Using the values for Z_2 and Z_3 in section 5, we obtain $g_{\text{MOM}}(\mu)$, which is shown in figure 8, or, equivalently, $\alpha_{\text{MOM}}(\mu)$, shown in figure 9. The coupling appears to reach a peak at about 1 GeV, below which it drops towards zero. However, caution is clearly warranted: the two or three lowest momentum points where this effect can be observed may well contain substantial finite volume effects (indeed, this was the case with the gluon propagator on the same lattice [13]), which only a simulation on a larger volume can resolve.

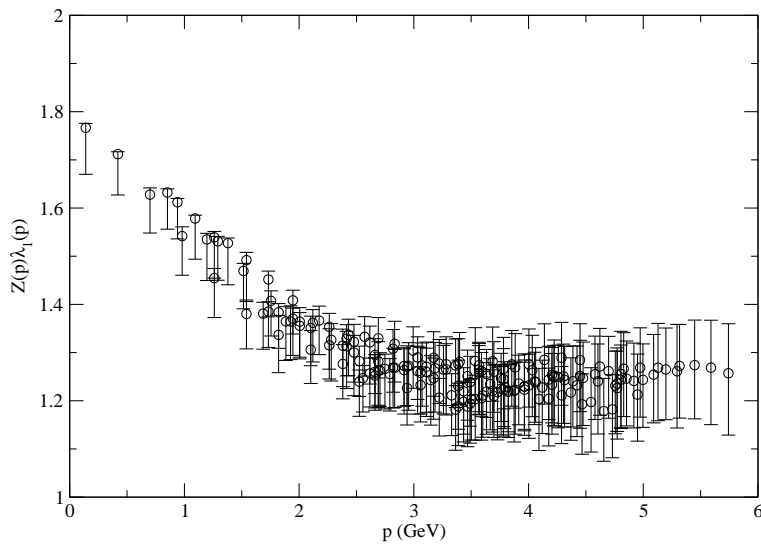


Figure 7: The unrenormalised form factor $\lambda_1(p^2, 0, p^2)$ multiplied by the quark renormalisation function $Z(p)$, using the improved propagator S_I , as a function of p .

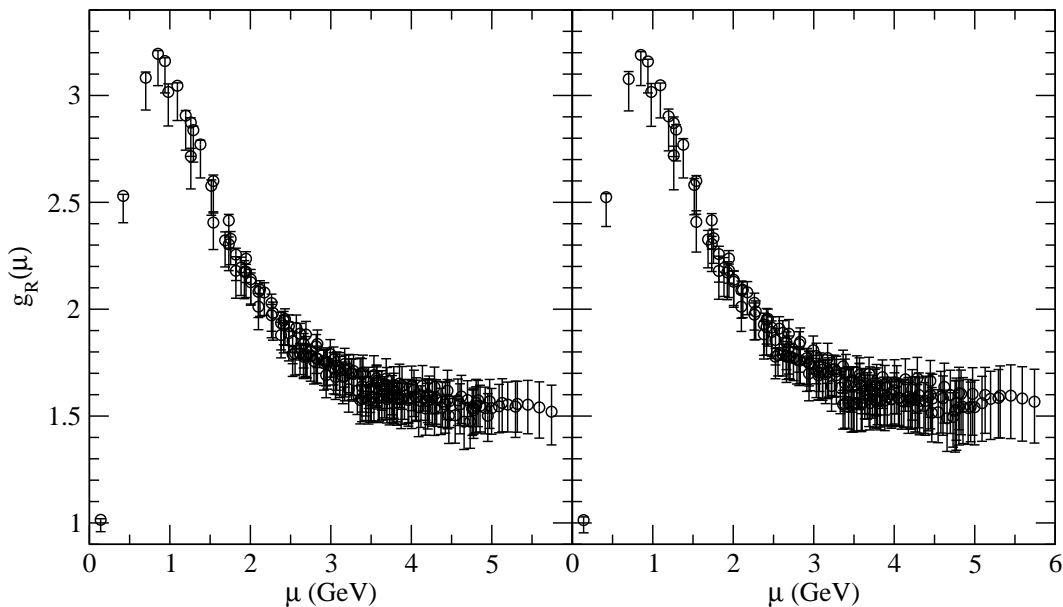


Figure 8: $g_{\widetilde{\text{MOM}}}(\mu)$ as a function of μ (GeV), using S_0 (left), and S_I (right).

Thus, at this point, we are not able to tell whether this may be a finite volume artefact, an artefact of the $\widetilde{\text{MOM}}$ scheme, or a real physical effect. Similarly, the fact that the peak value $\alpha_{\widetilde{\text{MOM}}} \sim 0.8$ is very close to typical values for the frozen coupling extracted from phenomenology [8], may be suggestive, but nothing more.

Turning now to the ultraviolet behaviour, we attempt to parametrise the leading non-perturbative and quark mass effects by fitting the results to the formula [39]

$$\alpha(\mu) \equiv \frac{g^2(\mu)}{4\pi} = \left(1 + \frac{c}{\mu^2}\right) \alpha^{2\text{loop}}(\mu), \quad (6.1)$$

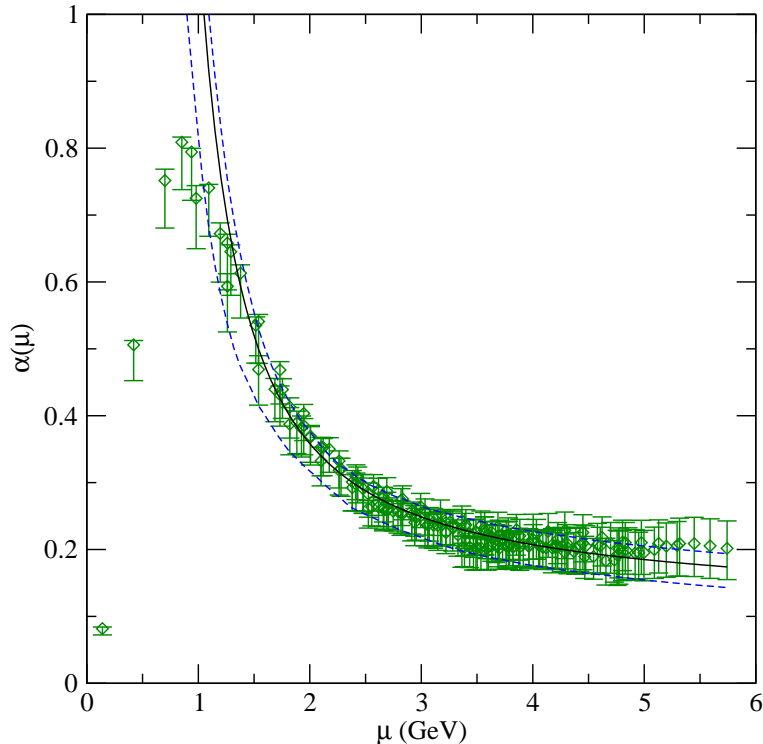


Figure 9: $\alpha_{\widetilde{\text{MOM}}}(\mu)$ as a function of μ (GeV). Also shown is the fit to (6.1) for $\mu > 2.0$ GeV.

for $\mu \geq p_{min}$, where $\alpha^{2\text{loop}}$ is the two-loop running coupling,

$$4\pi\alpha^{2\text{loop}}(\mu) = \frac{1}{b_0 \ln(\mu^2/\Lambda^2) + \frac{b_1}{b_0} \ln \ln(\mu^2/\Lambda^2)}, \quad (6.2)$$

with $b_0 = 11/16\pi^2$ and $b_1 = 102/(16\pi^2)^2$ the leading coefficients of the β -function, for varying values of p_{min} . The results are shown in table 1. In all cases, the numbers obtained using S_0 are almost identical to those obtained using S_I , so we only report the latter. We may also, if we ignore the power corrections (i.e., set $c = 0$), compute $\Lambda_{\widetilde{\text{MOM}}}$ directly according to the inverse of (6.2),

$$\Lambda = \mu e^{-\frac{1}{2b_0g^2(\mu)}} (b_0g^2(\mu))^{-\frac{b_1}{2b_0^2}}. \quad (6.3)$$

The results of this are shown in figure 10. The numbers obtained by fitting this to a constant above p_{min} are also reported in table 1. These numbers are consistent with the result of fitting $\alpha(\mu)$ to (6.2). We may also repeat this procedure after absorbing the power correction (6.1) in our definition of g_R , using the value for c from our fit. The result of this is also shown in figure 10 and reported in table 1.

In lattice studies of momentum-space quantities, the momentum variable is to some extent arbitrary. We may choose any of the variables p , $K(p)$, $Q(p)$, $\tilde{K}(p)$ or any other variable as long as it approaches p in the infrared and in the continuum limit, i.e. for $pa \ll 1$. If the continuum tree-level form of the quantity is momentum-dependent, we may use this

p_{min} (GeV)	n	Λ^0 (MeV)	$c(\text{GeV}^2)$	Λ (MeV)	Λ^r (MeV)
2.00	155	582^{+63}_{-128}	$1.4^{+2.4}_{-1.5}$	382^{+192}_{-232}	425^{+216}_{-259}
2.25	149	567^{+69}_{-135}	$1.1^{+2.6}_{-1.6}$	407^{+208}_{-250}	454^{+236}_{-276}
2.50	139	555^{+79}_{-141}	$0.6^{+2.9}_{-1.8}$	445^{+223}_{-272}	497^{+253}_{-305}
2.75	125	544^{+97}_{-157}	$0.3^{+3.3}_{-2.3}$	461^{+275}_{-304}	515^{+312}_{-341}
3.00	112	534^{+103}_{-169}	$-0.5^{+3.6}_{-2.4}$	523^{+331}_{-372}	586^{+376}_{-415}
3.25	101	528^{+114}_{-175}	$-1.7^{+4.2}_{-2.4}$	613^{+366}_{-410}	686^{+411}_{-456}
3.50	85	536^{+124}_{-182}	$-2.2^{+4.2}_{-2.4}$	662^{+386}_{-428}	740^{+434}_{-480}

Table 1: Fit parameters, using different momentum ranges. p_{min} denotes the lower end of the fit window; the maximum in all cases being the maximum total momentum 5.75 GeV. n is the number of momentum points used in the fit. Λ^0 is the value obtained for Λ_{MOM} without power correction, using (6.3), while Λ^r is the value obtained by using the fitted value for c to extract $\alpha^{2\text{loop}}$ and feeding this into (6.3).

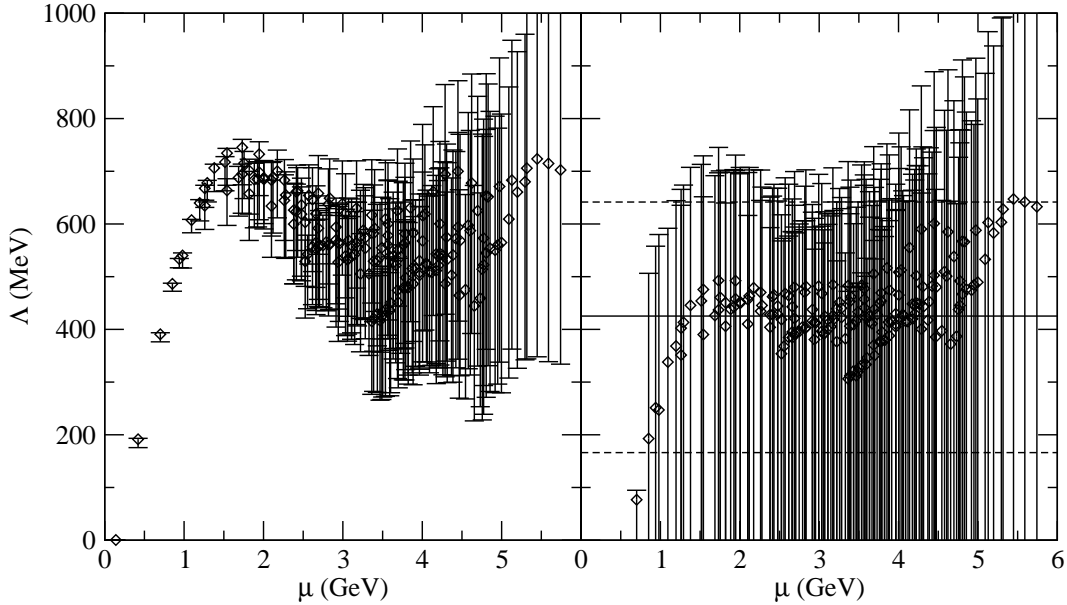


Figure 10: $\Lambda_{\text{MOM}}(\mu)$ (GeV) as a function of μ (GeV). Left: without power correction. Right: including the power correction of (6.1) from a fit to $\mu > 2.0$ GeV. The lines indicate the preferred value for Λ_{MOM} , with a 67% confidence interval.

to guide our choice of variable [14]; however, when it is not, the choice remains largely arbitrary [21]. Since the tree-level continuum vertex is momentum-independent, this is the situation we find ourselves in here. In order to quantify the resulting ambiguity, we have, in addition to the ‘naïve’ momentum p , performed fits using $K(p) \equiv \sqrt{\sum_{\mu} \sin^2(ap_{\mu})}/a$, which appears in the tree-level lattice vertex (B.12), as well as $K_z(p) \equiv K(p)/Z^{(0)}(p)$, which is the momentum variable that makes the tree-level quark propagator take its continuum form. The use of this variable may be justified because the correction factor $Z^{(0)}(p)$ appears also in the tree-level vertex, and also from the Ball–Chiu relation (2.22). The results of the fits are given in tables 2 and 3.

K_{min} (GeV)	n	Λ^0 (MeV)	$c(\text{GeV}^2)$	Λ (MeV)	Λ^r (MeV)
2.00	146	436^{+59}_{-109}	$0.4^{+2.2}_{-1.3}$	343^{+209}_{-221}	374^{+236}_{-242}
2.25	123	423^{+76}_{-121}	$-0.2^{+2.2}_{-1.3}$	404^{+246}_{-268}	443^{+275}_{-296}
2.50	101	423^{+90}_{-130}	$-0.2^{+3.3}_{-1.7}$	400^{+303}_{-309}	437^{+342}_{-340}
2.75	78	421^{+98}_{-141}	$-0.8^{+3.9}_{-1.8}$	464^{+336}_{-353}	511^{+376}_{-390}
3.00	46	425^{+130}_{-168}	$-3.0^{+3.0}_{-1.6}$	725^{+391}_{-463}	805^{+436}_{-518}
3.25	24	455^{+161}_{-190}	$-2.8^{+4.0}_{-2.4}$	699^{+496}_{-544}	780^{+553}_{-609}
3.50	9	470^{+189}_{-233}	$0.0^{+21.5}_{-5.5}$	421^{+813}_{-419}	468^{+910}_{-465}

Table 2: As table 1, using $K(p)$ as our momentum variable. The maximum available momentum here is 3.70 GeV.

$K_{z,min}$ (GeV)	n	Λ^0 (MeV)	$c(\text{GeV}^2)$	Λ (MeV)	Λ^r (MeV)
2.00	155	615^{+65}_{-134}	$1.1^{+2.0}_{-1.3}$	442^{+192}_{-233}	483^{+218}_{-259}
2.25	150	605^{+76}_{-145}	$1.1^{+2.1}_{-1.5}$	443^{+202}_{-241}	484^{+225}_{-266}
2.50	145	596^{+83}_{-149}	$0.8^{+2.1}_{-1.5}$	461^{+194}_{-258}	503^{+223}_{-283}
2.75	133	591^{+94}_{-164}	$1.3^{+2.6}_{-1.7}$	429^{+217}_{-257}	466^{+254}_{-283}
3.00	121	583^{+106}_{-172}	$1.9^{+3.2}_{-2.5}$	395^{+227}_{-257}	430^{+257}_{-281}
3.25	112	578^{+110}_{-177}	$2.2^{+4.3}_{-2.8}$	377^{+237}_{-237}	410^{+268}_{-260}
3.50	102	571^{+116}_{-184}	$2.4^{+5.0}_{-3.3}$	369^{+317}_{-257}	402^{+356}_{-271}

Table 3: As table 1, using $K_z(p)$ as our momentum variable. The maximum available momentum here is 5.05 GeV.

From figure 9 and the right-hand panel of figure 10 it would appear that the data are very well represented by a power-corrected two-loop running coupling as in (6.1), all the way down to 1.5 GeV if not lower. However, a glance at tables 1–3 reveals several problems with this.

Firstly, the fits are nowhere near stable. As the starting point for the fits goes from 2.5 to 3.5 GeV, the best value for Λ increases by 50% when using p as our momentum variable, and the power correction goes from positive to negative. Secondly, the ‘refitted’ value for Λ , although always perfectly consistent with that obtained from (6.1), is consistently about 10% higher.

Thirdly, the fit values depend critically on which momentum value is used. To some extent this is simply because the values of p , $K(p)$, and $K_z(p)$ may be very different when $pa \gg 1$, so different data are included in the fits. This is reflected in the different number of points for the same numerical value of the starting momentum. However, it also reflects a deeper ambiguity due to the finite lattice spacing. I.e., although there is no violation of $O(4)$ symmetry or other obvious signs of lattice artefacts in our data, and the near-perfect agreement between the S_0 and S_I results may be taken as an indication that lattice spacing errors are very small, those errors that do persist make a determination of a sensitive quantity such as $\Lambda_{\widetilde{\text{MOM}}}$ prone to large uncertainties. It should be noted that we observe considerable anisotropy in the high-momentum region when g_R is plotted as a

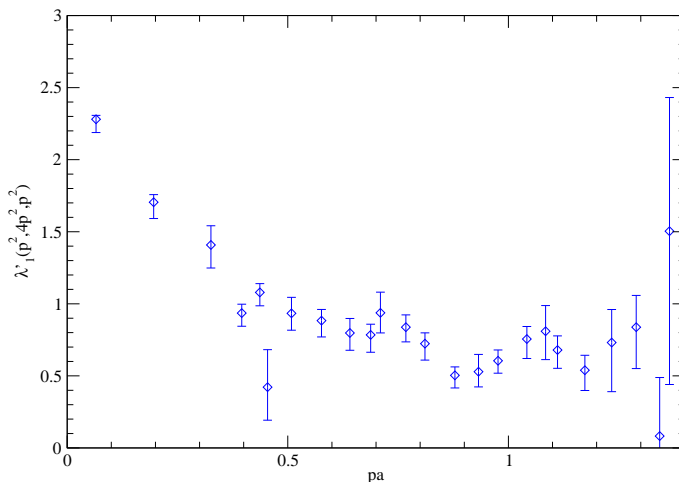


Figure 11: The unrenormalised, tree-level corrected form factor $\lambda'_1(p^2, 4p^2, p^2)$ as a function of the quark momentum $|pa|$, from 498 configurations.

function of $K(p)$ or $K_z(p)$ as opposed to p , indicating that these are not the appropriate momentum variables in this case. Only by repeating the simulation at a smaller lattice spacing can this issue be properly resolved, however.

Taking all this into account, we take as our best estimate for Λ the average of all the fits starting from 3.0 GeV (both with and without the power correction). This gives $\Lambda_{\overline{\text{MOM}}} = 530_{-320}^{+260} \pm 100 \pm 50$ MeV, where the first set of errors are statistical, the second are due to the ambiguities in the choice of momentum variable, and the third is the intrinsic 10% systematic uncertainty in the lattice spacing in the quenched approximation.

6.2 Symmetric scheme

At the symmetric point $2p + q = 0$ we use only the improved propagator S_I , and thus the form factor λ'_1 receives substantial tree-level correction according to (B.25)–(B.28). The tree-level corrected result is shown in figure 11. In order to reduce the statistical noise, we have averaged data for nearby momenta, within $\Delta pa < 0.05$. We see that the data are still considerably more noisy than for the asymmetric λ_1 of figure 6, but exhibit qualitatively the same behaviour. It appears that $\lambda'_1(p^2, 4p^2, p^2)$ is more strongly infrared enhanced than $\lambda_1(p^2, 0, p^2)$, but the noise makes it difficult to draw any definite conclusion.

The $\overline{\text{MOM}}$ running coupling $g_{\overline{\text{MOM}}}(\mu)$ is shown as a function of the renormalisation scale μ in figure 12. The most obvious difference from the $\overline{\text{MOM}}$ coupling of figure 8 is that the noise is far worse, and we are not able to get any signal for Λ from these data.

7. Matching to $\overline{\text{MS}}$

The relation between the scale parameters in two renormalisation schemes A and B is given by [1]

$$\frac{\Lambda_A}{\Lambda_B} = \exp\left[-\frac{C_{AB}}{2b_0}\right], \quad (7.1)$$

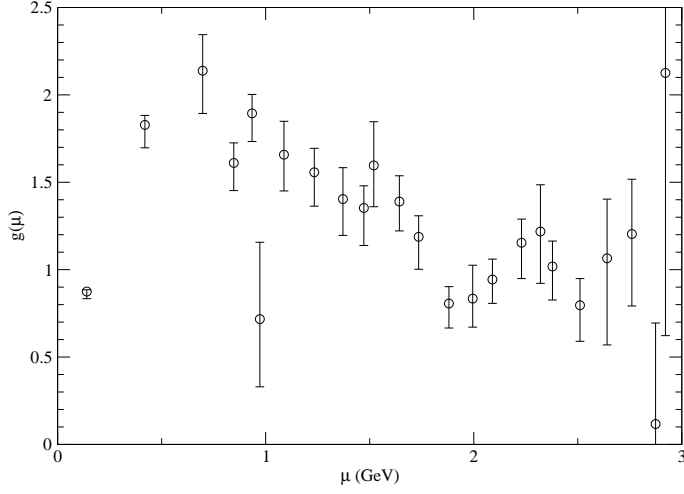


Figure 12: $g_{\text{MOM}}(\mu)$ as a function of μ (GeV).

where C_{AB} is the one-loop coefficient in the expansion of the coupling g_B^2 in terms of g_A^2 .

The complete one-loop expressions for the relevant form factors in the two kinematics we are studying, are given in appendix C. Here we only reproduce the results for the running coupling in Landau gauge, for $N_f = 0$. The $\overline{\text{MOM}}$ coupling is given by

$$g_{\overline{\text{MOM}}}(\mu) = g_{\overline{\text{MS}}}(\mu) \left[1 + \left(\frac{151}{24} - \frac{3m^2}{4\mu^2} - \frac{9}{4} \ln\left(1 + \frac{m^2}{\mu^2}\right) + \frac{m^2}{\mu^2} \ln\left(1 + \frac{\mu^2}{m^2}\right) \left[\frac{4}{3} + \frac{25m^2}{12\mu^2} \right] \right) \frac{g_{\overline{\text{MS}}}^2(\mu)}{16\pi^2} + \mathcal{O}(g^4) \right]. \quad (7.2)$$

However, at asymptotically large momenta, where one-loop perturbation theory becomes valid, the corrections due to the mass term can be ignored. From (7.1) we thus find that

$$\frac{\Lambda_{\overline{\text{MOM}}}}{\Lambda_{\overline{\text{MS}}}} = \exp \frac{151}{264} = 1.77. \quad (7.3)$$

Using our ‘best value’ for $\Lambda_{\overline{\text{MOM}}}$, we obtain

$$\Lambda_{\overline{\text{MS}}}^{N_f=0} = 300_{-180}^{+150} \pm 55 \pm 30 \text{ MeV}. \quad (7.4)$$

These numbers are above those obtained by other methods [6, 29], which yield a ‘world average’ of $\Lambda_{\overline{\text{MS}}}^{N_f=0} = 240(10)$ MeV. With our large statistical and systematic uncertainties, our value is however fully consistent with the ‘world average’.

The $\overline{\text{MOM}}$ coupling in the massless limit is

$$g_{\overline{\text{MOM}}}(\mu) = g_{\overline{\text{MS}}}(\mu) \left\{ 1 + \left(\frac{4}{9} \ln 2 + \frac{793}{72} \right) \frac{g_{\overline{\text{MS}}}(\mu)}{16\pi^2} + \mathcal{O}(g^4) \right\}, \quad (7.5)$$

which gives for $\Lambda_{\overline{\text{MOM}}}$

$$\frac{\Lambda_{\overline{\text{MOM}}}}{\Lambda_{\overline{\text{MS}}}} = \exp \left(\frac{8 \ln 2/9 + 793/36}{22} \right) = 2.80. \quad (7.6)$$

If, instead, we renormalise the vertex at the gluon momentum, we find

$$\frac{\Lambda_{\text{MOM}}^g}{\Lambda_{\overline{\text{MS}}}} = \exp\left(\frac{89 \ln 2/9 + 793/36}{22}\right) = 3.72. \quad (7.7)$$

8. Discussion and outlook

We have studied the quark-gluon vertex in the Landau gauge, in quenched QCD with $\mathcal{O}(a)$ -improved Wilson fermions, at two different kinematical points: an ‘asymmetric’ point, where the gluon momentum q is zero, and a ‘symmetric’ point, where $q = -2p$, in other words the incoming quark has equal and opposite momentum to the outgoing quark.

We have focused on the form factor λ_1 , which is proportional to the running coupling and, in the decomposition given by (A.6), (A.8), is the only form factor that is expected to be ultraviolet divergent. At the symmetric point, we are unable to study this form factor directly, and examine instead the linear combination $\lambda'_1 \equiv \lambda_1 - q^2 \tau_3$. We observe that in both kinematics, $\lambda_1(\lambda'_1)$ is substantially enhanced in the infrared. At the asymmetric point, this enhancement is significantly stronger than that expected in QED due to the well-established enhancement of the quark propagator form factor $A(p)$. At the asymmetric point, no such direct comparison with QED is possible due to the admixture of τ_3 , which is left unconstrained by the Ward–Takahashi (or Slavnov–Taylor) identity. However, the qualitative picture is the same.

The lattice volume in this study is relatively small (a spatial length of ~ 1.5 fm and a total volume of 15–16 fm⁴), so the infrared behaviour may well be contaminated by substantial finite volume effects. Although we have explicitly accounted for the large finite-volume effects appearing in the tensor structure of the gluon propagator, we have no guarantee that there are not substantial residual effects that, at the asymmetric point, could play an important role for all momenta. However, excellent agreement with results for $\Lambda_{\overline{\text{MS}}}$ obtained by other methods have been obtained from the three-gluon vertex in a $\widetilde{\text{MOM}}$ scheme on symmetric lattices [29], and there appears to be no reason why the situation should be much worse in our case. The qualitative similarity between the symmetric and asymmetric point might also be taken as an indication that finite volume effects, although possibly sizeable, do not dominate. In any case, it would be desirable to perform the simulation on a larger lattice in order to have a better resolution of the momentum in directions other than the time direction. This is also the only way we would be able to settle the issue of whether the running coupling is frozen, or possibly goes to zero.

We have used the results for λ_1 at the asymmetric point to determine the running coupling α_s in a zero-momentum ($\widetilde{\text{MOM}}$) renormalisation scheme, and obtained from this a nonperturbative estimate of $\Lambda_{\overline{\text{MS}}}^{N_f=0}$. Our main results are for the strong coupling $\alpha_{\widetilde{\text{MOM}}}^{N_f=0}(2\text{GeV}) = 0.36(4)$; $\alpha_{\overline{\text{MS}}}^{N_f=0}(2\text{GeV}) = 0.28(3)$, and for the QCD scale $\Lambda_{\overline{\text{MS}}}^{N_f=0} = 300_{-180}^{+150} \pm 55 \pm 30$ MeV, where the first set of errors are statistical, the second due to ambiguities in defining the momentum variable, and the third due to uncertainty in the lattice spacing. This is consistent with, although slightly higher than other estimates for $\Lambda_{\overline{\text{MS}}}$.

Although the excellent agreement between the results using the ‘unimproved’ propagator S_0 and the ‘improved’ propagator S_I indicate that our tree-level correction scheme has successfully accounted for the large high-momentum lattice artefacts, and that residual $\mathcal{O}(a)$ errors are not a significant factor, the need for large tree-level corrections still implies some uncertainty about the results, at least in the intermediate momentum regime. A fermion action which is more well-behaved at high momenta, such as overlap fermions, would be a great improvement.

The main source of systematic uncertainty, and of possible discrepancies between our result for $\Lambda_{\overline{\text{MS}}}^{N_f=0}$ and those of other determinations, is that we have not been able to access sufficiently high momenta, where two-loop scaling should be valid, nor have we taken into account higher-order perturbative effects, which should extend the range of validity for the perturbative matching. Experience from the 3-gluon vertex [29] suggests that both a large momentum window and 3-, perhaps 4-loop running of the β -function are needed to obtain reliable results. This requires simulations at smaller lattice spacings, as well as a two-loop calculation of the λ_1 form factor in the relevant kinematical limit. Both are computationally very expensive.

As we mentioned in the introduction, two-loop calculations have already been performed in both an asymmetric [4] and a symmetric [5] kinematics. Neither is, however, the kinematics we are employing here.

In the $\overline{\text{MOM}}$ (symmetric) kinematics, we have been unable to get a reasonable signal for the running coupling. The main reason for this is statistical noise, but the need for large tree-level corrections is clearly also a significant factor. For this reason it would be essential, if we were to attempt a more accurate determination of the vertex in this kinematics, to choose a fermion discretisation which is not afflicted by such problems.

In a precision study, the quark mass must also be handled carefully. Here, we have merely included the quark mass in the overall power correction, which has been determined numerically. An obvious next step would be to study the vertex at a second quark mass. It would be an advantage, also for this purpose, to use a fermion action which respects chiral symmetry, such as overlap fermions, or a remnant thereof, such as staggered fermions.

The large numerical uncertainties have prevented us from obtaining any reliable estimate of the power correction. An alternative approach would be to calculate analytically the size of the power corrections from the condensates involved, of which the dominant is expected to be the chiral condensate, using the available estimates for the values of the condensates.

The running coupling extracted in the $\widetilde{\text{MOM}}$ scheme reaches a maximum at 0.8 GeV. A similar result was found for the three-gluon vertex in an analogous $\widehat{\text{MOM}}$ scheme [28, 29]. This would correspond to a zero in the β -function at the maximum coupling, with double values below that. It has been suggested [40] that this can be related to infrared singularities in the ghost self-energy. Such singularities should not affect symmetric momentum subtraction schemes. Our results in the $\overline{\text{MOM}}$ scheme can neither confirm nor refute this conjecture.

In order to resolve this issue, and to pin down the low- and intermediate-momentum behaviour of the quark–gluon vertex, simulations on larger, and possibly coarser lattices

are necessary. This is an orthogonal line of inquiry to that needed to determine the running coupling along with the power corrections, which requires much finer, but not larger lattices.

Work is currently in progress to determine the form factors λ_2 and λ_3 at the asymmetric ($q = 0$) point. These form factors both vanish at tree level in the continuum, but must be non-zero nonperturbatively in order to fulfil the Slavnov–Taylor identity. A complete determination of all form factors would be a natural next step. This is, however, not possible in Landau gauge because of the transversality condition. For this reason, and also because the gauge dependence of the vertex is in itself of theoretical importance, it would be of great interest to study the vertex in a generic covariant gauge [41, 42]. This would also allow calculations in the unmodified symmetric $\overline{\text{MOM}}$ scheme, which might have some advantages over the modified scheme we have used here.

At present, there is no known method to reliably assess the effect of Gribov copies. All numerical methods founder on the fact that as the physical volume increases, the number of Gribov copies also increases, and it becomes impossible to ascertain that one has found either the absolute maximum of the gauge fixing functional, or any other unique representative. Choosing a gauge without Gribov copies, such as the Laplacian gauge [43] or axial gauges, does not solve the problem, since results in one gauge tell us nothing about the effect of Gribov copies in a different gauge.

On a practical level, attempting to select, however imperfectly, the absolute maximum, using e.g. ‘brute force’ [24], simulated annealing [16], or smeared gauge fixing [44] is in principle worthwhile. At present, however, we would expect any signal showing a difference between the naïve (minimal) Landau gauge and the fundamental modular domain to be swamped by statistical noise for three-point functions such as the quark–gluon vertex.

Acknowledgments

We wish to give special thanks to Tony Williams for numerous long and productive discussions and a careful reading of the manuscript. We also thank Claudio Parrinello, Derek Leinweber, Reinhard Alkofer, Peter Watson and Olivier Pène for stimulating discussions and advice. We acknowledge support from the Norwegian Research Council, the Australian Research Council, the European Union TMR network “Finite temperature phase transitions in particle physics”, and FOM (The Netherlands). This study was performed using UKQCD configurations, produced on a Cray T3D based at EPCC, University of Edinburgh, using UKQCD Collaboration CPU time under PPARC Grant GR/K41663.

A. Tensor decomposition of the vertex

The Lorentz structure of the vertex in the continuum consists of 12 independent vectors and can be written as

$$\Lambda_\mu \equiv -ig_0\Gamma_\mu = -ig_0 \sum_{i=1}^{12} f_i F_\mu^i, \quad (\text{A.1})$$

where

$$\begin{aligned}
F_\mu^1 &= p_\mu & ; & & F_\mu^2 &= q_\mu & ; & & F_\mu^3 &= \gamma_\mu & ; & & F_\mu^4 &= \not{p} p_\mu ; \\
F_\mu^5 &= \not{p} q_\mu & ; & & F_\mu^6 &= \not{q} p_\mu & ; & & F_\mu^7 &= \not{q} q_\mu & ; & & F_\mu^8 &= \not{p} \gamma_\mu ; \\
F_\mu^9 &= \not{q} \gamma_\mu ; & & & F_\mu^{10} &= \not{p} \not{q} p_\mu ; & & & F_\mu^{11} &= \not{p} \not{q} q_\mu ; & & & F_\mu^{12} &= \not{p} \not{q} \gamma_\mu .
\end{aligned} \tag{A.2}$$

It is useful to divide the vertex into a ‘Slavnov–Taylor’ (non-transverse) part and a transverse part, as is commonly done in QED:

$$\Lambda_\mu(p, q) = \Lambda_\mu^{(ST)}(p, q) + \Lambda_\mu^{(T)}(p, q) . \tag{A.3}$$

The ST part is that part of the vertex that saturates the Slavnov–Taylor identity (1.2) and contains no kinematical singularities. It is often, misleadingly, referred to as the ‘longitudinal’ part, although it also contains a transverse component.

We will make use of the QED decomposition [3, 26, 27] of the fermion–gauge-boson vertex function, which is usually given in Minkowski space. We wish to write the euclidean-space equivalent, in such a way that all the scalar form factors λ_i and τ_i are the same as in Minkowski space. The usual procedure is to apply the Wick rotation ($p_0 \rightarrow ip_4, p_i \rightarrow -p_i, \gamma_0 \rightarrow \gamma_4, \gamma_i \rightarrow i\gamma_i$), but since the vertex is a four-vector, this is not a linear transformation in our case. Our prescription is to create a Lorentz scalar by contracting the vertex with γ_μ and require that the Wick-rotated Minkowski result is identical to what we obtain by performing this operation in euclidean space. In particular, any euclidean scalar function should be equal to the Minkowskian scalar function sampled at spacelike (i.e. negative) momenta:

$$f_E(p^2, q^2, k^2) \equiv f_M(-p^2, -q^2, -k^2) , \tag{A.4}$$

where f can be τ_i or λ_i .

Following this prescription, we can write the ST part as [with $k = p + q$]

$$\Lambda_\mu^{(ST)}(p, q) = -ig \sum_{i=1}^4 \lambda_i(p^2, q^2, k^2) L_{i,\mu}(p, q) , \tag{A.5}$$

where the euclidean-space functions $L_{i,\mu}$ are given by

$$\begin{aligned}
L_{1,\mu} &= \gamma_\mu & ; & & L_{2,\mu} &= -(2 \not{p} + \not{q})(2p + q)_\mu ; \\
L_{3,\mu} &= -i(2p + q)_\mu ; & & & L_{4,\mu} &= -i\sigma_{\mu\nu}(2p + q)_\nu .
\end{aligned} \tag{A.6}$$

For the purely transverse part $\Lambda^{(T)}$, we will use the decomposition of [27], which differs slightly from the one of [3, 26]. This decomposition is preferable because it is free of kinematical singularities in all covariant gauges. Moreover, as we shall see, the relation between the ST and purely transverse parts of the vertex becomes more transparent in this basis. The purely transverse part of the vertex is specified by $q_\mu \Lambda_\mu^{(T)}(p, q) = 0$ and satisfies $\Lambda_\mu^{(T)}(p, 0) = 0$, and we write

$$\Lambda_\mu^{(T)}(p, q) = -ig \sum_{i=1}^8 \tau_i(p^2, q^2, k^2) T_{i,\mu}(p, q) , \tag{A.7}$$

where the euclidean-space functions T_i are given by

$$\begin{aligned}
T_{1,\mu} &= i [p_\mu q^2 - q_\mu (p \cdot q)] ; \\
T_{2,\mu} &= [p_\mu q^2 - q_\mu (p \cdot q)] (2 \not{p} + \not{q}) ; \\
T_{3,\mu} &= \not{q} q_\mu - q^2 \gamma_\mu ; \\
T_{4,\mu} &= -i [q^2 \sigma_{\mu\nu} (2p + q)_\nu + 2q_\mu \sigma_{\nu\lambda} p_\nu q_\lambda] ; \\
T_{5,\mu} &= -i \sigma_{\mu\nu} q_\nu ; \\
T_{6,\mu} &= q \cdot (2p + q) \gamma_\mu - \not{q} (2p + q)_\mu ; \\
T_{7,\mu} &= \frac{i}{2} q \cdot (2p + q) [(2 \not{p} + \not{q}) \gamma_\mu - (2p + q)_\mu] - i (2p + q)_\mu \sigma_{\nu\lambda} p_\nu q_\lambda ; \\
T_{8,\mu} &= -\gamma_\mu \sigma_{\nu\lambda} p_\nu q_\lambda - \not{p} q_\mu + \not{q} p_\mu .
\end{aligned} \tag{A.8}$$

Charge conjugation symmetry dictates that all the λ_i 's and τ_i 's are even with respect to interchanges of p^2 and k^2 (or $(p + q)^2$), except for λ_4, τ_4 and τ_6 , which are odd.

In this decomposition, the transverse projection of the ST part of the vertex is given by

$$P_{\mu\nu}(q) L_{1,\nu}(p, q) = -\frac{1}{q^2} T_{3,\mu}(p, q) ; \tag{A.9}$$

$$P_{\mu\nu}(q) L_{2,\nu}(p, q) = -\frac{2}{q^2} T_{2,\mu}(p, q) ; \tag{A.10}$$

$$P_{\mu\nu}(q) L_{3,\nu}(p, q) = -\frac{2}{q^2} T_{1,\mu}(p, q) ; \tag{A.11}$$

$$P_{\mu\nu}(q) L_{4,\nu}(p, q) = \frac{1}{q^2} T_{4,\mu}(p, q) . \tag{A.12}$$

Thus, we will define the following modified form factors, which appear in the transverse-projected vertex:

$$\begin{aligned}
\lambda'_1 &= \lambda_1 - q^2 \tau_3 ; & \lambda'_2 &= \lambda_2 - \frac{q^2}{2} \tau_2 ; \\
\lambda'_3 &= \lambda_3 - \frac{q^2}{2} \tau_1 ; & \lambda'_4 &= \lambda_4 + q^2 \tau_4 .
\end{aligned} \tag{A.13}$$

B. Tree-level lattice expressions

We define and use the following momentum variables, which may be used to bring the lattice tree-level expressions into a more continuum-like form,

$$K_\mu(p) \equiv \frac{1}{a} \sin(p_\mu a) , \tag{B.1}$$

$$Q_\mu(p) \equiv \frac{2}{a} \sin(p_\mu a/2) = \frac{\sqrt{2}}{a} \sqrt{1 - \cos(p_\mu a)} , \tag{B.2}$$

$$\tilde{K}_\mu(p) \equiv \frac{1}{2} K_\mu(2p) = \frac{1}{2a} \sin(2p_\mu a) , \tag{B.3}$$

$$C_\mu(p) \equiv \cos(p_\mu a) . \tag{B.4}$$

At tree level, the dimensionless momentum-space propagator $S_0(p)$ is identical to the free Wilson propagator,

$$S_0^{(0)}(p) = \frac{-ia \mathcal{K}(p) + ma + \frac{1}{2}a^2Q^2(p)}{a^2K^2(p) + (ma + \frac{1}{2}a^2Q^2(p))^2}. \quad (\text{B.5})$$

The tree-level form of the $\mathcal{O}(a)$ -improved propagator S_I is given by

$$S_I^{(0)}(p) = (1 + b_q am)S_0^{(0)}(p) - 2ac'_q = \frac{Z^{(0)}(p)}{ia \mathcal{K}(p) + amZ_m^{(0)}(p)}, \quad (\text{B.6})$$

where

$$Z^{(0)}(p) = \frac{1 + b_q am}{D_I(p)} \left[K^2(p) + \left(m + \frac{1}{2}Q^2(p)\right)^2 \right], \quad (\text{B.7})$$

with

$$D_I(p) = (1 + b_q am)^2 K^2(p) + B_I^2(p), \quad (\text{B.8})$$

$$B_I(p) = (1 + b_q am) \left(m + \frac{1}{2}Q^2(p)\right) - 2ac'_q \left[K^2(p) + \left(m + \frac{1}{2}Q^2(p)\right)^2 \right]. \quad (\text{B.9})$$

The tree-level functions $Z^{(0)}$ and $Z_m^{(0)}$ (which is given in [19] and will not be reproduced here) give rise to very large finite- a effects at intermediate and large momenta. To reduce these lattice artefacts, and bring the high-momentum behaviour of the quark propagator into contact with the continuum perturbative behaviour, we employ the tree-level correction scheme defined in [18, 19], where the quark propagator is written as

$$S^{-1}(p) = \frac{1}{Z(p)Z^{(0)}(p)} \left[ia \mathcal{K}(p) + aM^h(p)Z_m^{(+)}(p) + a\Delta M^{(-)}(p) \right], \quad (\text{B.10})$$

with the functions $Z^{(0)}$, $Z_m^{(+)}$ and $\Delta M^{(-)}$ denoting the tree-level behaviour. We call the functions $Z(p)$ and $M^h(p)$ the tree-level corrected quark form factors. Here, we are only interested in $Z(p)$, which can be related to the quark field renormalisation constant Z_2 , so we can ignore the mass correction functions $Z_m^{(+)}$, $\Delta M^{(-)}$ which are defined in [19].

At tree level, the Landau gauge gluon propagator becomes

$$D_{\mu\nu}(q) = P_{\mu\nu}^{\text{lat}}(q)D(Q^2) = \left(\delta_{\mu\nu} - \frac{Q_\mu(q)Q_\nu(q)}{Q^2(q)} \right) \frac{1}{Q^2(q)}. \quad (\text{B.11})$$

In this notation, the gluon propagator requires no further tree-level correction.

The tree-level lattice vertex using the ‘unimproved’ propagator S_0 is [45, 46]

$$\Lambda_{0,\mu}^{a(0)}(p, q) = -ig_0 t^a \left(\gamma_\mu \cos \frac{a(2p+q)_\mu}{2} - i \sin \frac{a(2p+q)_\mu}{2} - i \frac{c_{\text{sw}}}{2} \sum_\nu \sigma_{\mu\nu} \cos \frac{aq_\mu}{2} \sin aq_\nu \right). \quad (\text{B.12})$$

The constant term c'_q in S_I does not contribute to the unamputated vertex V_μ in (2.4), since $\langle A_\mu \rangle = 0$. Thus, the improved vertex at tree level is given by

$$\Lambda_{I,\mu}^{a(0)}(p, q) = (1 + b_q am) S_I^{(0)}(p)^{-1} S_0^{(0)}(p) \Lambda_{0,\mu}^{a(0)}(p, q) S_0^{(0)}(p+q) S_I^{(0)}(p+q)^{-1}. \quad (\text{B.13})$$

The full expression is very complicated, but it simplifies greatly for the two cases (symmetric and asymmetric) in which we are interested.

B.1 Asymmetric kinematics

In this case the gluon momentum $q = 0$, while the quark momentum is ‘orthogonal’ to the vertex, i.e. the μ -component p_μ of the quark momentum is zero. Then the tree-level lattice vertex (B.12) reduces to

$$\Lambda_{0,\mu}^{a(0)}(p, 0) = -ig_0 t^a \gamma_\mu. \quad (\text{B.14})$$

Making use of this, along with the unimproved (B.5) and improved (B.6) propagators, the improved vertex (B.13) becomes

$$\begin{aligned} \Lambda_{I,\mu}^{a(0)}(p, 0)|_{p_\mu=0} &= (1 + b_q am) S_I^{(0)}(p)^{-1} S_0^{(0)}(p) \Lambda_{0,\mu}^{a(0)}(p, 0) S_0^{(0)}(p) S_I^{(0)}(p)^{-1} \\ &= -ig_0 t^a \gamma_\mu / Z^{(0)}(p). \end{aligned} \quad (\text{B.15})$$

Thus, at this point, the tree-level corrected vertex may be defined according to

$$\Lambda_{I,\mu}^a(p, 0)|_{p_\mu=0} = -it^a \frac{1}{Z^{(0)}(p)} g_0 \lambda_1(p^2, 0, p^2) \gamma_\mu. \quad (\text{B.16})$$

As previously mentioned, in the Landau gauge we calculate the transverse-projected vertex (2.12). In the asymmetric case, this becomes

$$P_{\mu\nu}(q) \Lambda_\nu(p, q=0) = \delta_{\mu\nu} \Lambda_\nu^{(ST)}(p, 0) + \Lambda_\mu^{(T)}(p, 0) = \Lambda_\mu^{(ST)}(p, 0), \quad (\text{B.17})$$

since $\Lambda_\mu^{(T)}(p, 0) = 0$ and $P_{\mu\nu}(0) = \delta_{\mu\nu}$ as discussed on p. 5. The lattice, finite-volume version of this is

$$T_{\mu\nu}(q) \Lambda_\nu(p, q=0) |_{p_\mu=0} = T_{\mu\mu}(0) \Lambda_\mu^{(ST)}(p, 0) |_{p_\mu=0} = -i \frac{T_{\mu\mu}(0)}{Z^{(0)}(p)} g_0 \lambda_1(p^2, 0, p^2) \gamma_\mu. \quad (\text{B.18})$$

B.2 Symmetric kinematics

The second case we consider is the (symmetric) case where $2p + q = 0$, i.e. $p = -k$ or equivalently $q = -2p$. In this limit, the tree-level vertex (B.12) becomes (for ease of notation we will here set the lattice spacing $a = 1$)

$$\Lambda_{0,\mu}^{a(0)}(p, -2p) \equiv -ig_0 \Gamma_{0,\mu}^{a(0)}(p, -2p) = -ig_0 t^a \left(\gamma_\mu + ic_{\text{sw}} \sum_\nu \sigma_{\mu\nu} C_\mu(p) \tilde{K}_\nu(p) \right), \quad (\text{B.19})$$

and repeating the same procedure as in the asymmetric case, the improved vertex (B.13) takes the form

$$\Lambda_{I,\mu}^{a(0)}(p, -2p) = (1 + b_q m) S_I^{(0)}(p)^{-1} S_0^{(0)}(p) \Lambda_{0,\mu}^{a(0)}(p, -2p) S_0^{(0)}(-p) S_I^{(0)}(-p)^{-1}. \quad (\text{B.20})$$

This gives us

$$\begin{aligned}
\frac{D_I^2}{1+b_q m} \Gamma_{I,\mu}^{(0)}(p, -2p) &= \left[B_V^2 - A_V^2 K^2 + 2A_V B_V c_{\text{sw}}(K \cdot \tilde{K}) C_\mu \right] \gamma_\mu + 2A_V^2 K K_\mu \\
&\quad - 2A_V B_V c_{\text{sw}} \tilde{K} \tilde{K}_\mu - 2iA_V B_V \sum_\nu \sigma_{\mu\nu} K_\nu + ic_{\text{sw}}(A_V^2 K^2 + B_V^2) C_\mu \sum_\nu \sigma_{\mu\nu} \tilde{K}_\nu \\
&\quad - 2ic_{\text{sw}} A_V^2 (K \cdot \tilde{K}) \tilde{K}_\mu + 2ic_{\text{sw}} A_V^2 (K \cdot \tilde{K}) C_\mu K \gamma_\mu - 2ic_{\text{sw}} A_V^2 \tilde{K}_\mu \sum_{\nu\lambda} \sigma_{\nu\lambda} K_\nu \tilde{K}_\lambda, \quad (\text{B.21})
\end{aligned}$$

where we have written $K = K(p)$, $\tilde{K} = \tilde{K}(p)$, $C = C(p)$ and

$$A_V \equiv A_V(p) = (1 + b_q m) \left(m + \frac{1}{2} Q^2(p) \right) - B_I(p), \quad (\text{B.22})$$

$$B_V \equiv B_V(p) = (1 + b_q m) K^2(p) + \left(m + \frac{1}{2} Q^2(p) \right) B_I(p). \quad (\text{B.23})$$

If we concentrate on the part of this that becomes proportional to λ_1 and τ_3 in the continuum, the lattice expression may be decomposed as

$$\Gamma_{I,\mu}^{(0)}(p, -2p) = \lambda_1^{(0)} \gamma_\mu - 4\tau_3^{(0)} (K^2 \gamma_\mu - K K_\mu) - 4\tilde{\tau}_3^{(0)} (K \cdot \tilde{K} C_\mu \gamma_\mu - \tilde{K} \tilde{K}_\mu) + \dots \quad (\text{B.24})$$

We can read off the tree-level form factors from (B.21),

$$\lambda_1^{(0)}(p^2, 4p^2, p^2) = \frac{1 + b_q m}{D_I(p)^2} \left(A_V^2(p) K^2(p) + B_V^2(p) \right) = 1/Z^{(0)}(p); \quad (\text{B.25})$$

$$\tau_3^{(0)}(p^2, 4p^2, p^2) = \frac{1 + b_q m}{2D_I^2(p)} A_V^2(p); \quad (\text{B.26})$$

$$\tilde{\tau}_3^{(0)}(p^2, 4p^2, p^2) = -\frac{1 + b_q m}{2D_I^2(p)} c_{\text{sw}} A_V(p) B_V(p). \quad (\text{B.27})$$

As in the asymmetric case, we compute the transverse-projected vertex (2.12) in Landau gauge. With the decomposition (B.24), it reads (for sufficiently large q)

$$\begin{aligned}
\Gamma_\mu^P(p, -2p) &\equiv P_{\mu\nu}^{\text{lat}}(q) \Gamma_\nu(p, q = -2p) = \left(\delta_{\mu\nu} - \frac{Q_\mu(2p) Q_\nu(2p)}{Q^2(2p)} \right) \Gamma_\nu(p, -2p) \\
&= \left(\delta_{\mu\nu} - \frac{K_\mu(p) K_\nu(p)}{K^2(p)} \right) \Gamma_\nu(p, -2p) \\
&= \left(\lambda_1/K^2 - 4\tau_3 \right) (K^2 \gamma_\mu - K K_\mu) - 4\tilde{\tau}_3 (K \cdot \tilde{K} C_\mu \gamma_\mu - \tilde{K} \tilde{K}_\mu) + \dots \quad (\text{B.28})
\end{aligned}$$

This is the lattice equivalent of the projection (2.24). From this we obtain the transverse-projected, lattice equivalent of (3.7),

$$\begin{aligned}
h_1(4p^2) &= -\frac{1}{4} \sum_\mu \text{Im Tr } \gamma_\mu \Lambda_\mu^T(p, -2p) \\
&= 3g_0 \left(\lambda_1(p^2, 4p^2, p^2) - 4K^2 \tau_3(p^2, 4p^2, p^2) \right) \\
&\quad - 4g_0 \left(4K \cdot \tilde{K} - \tilde{K}^2 - \frac{1}{2} Q^2 K \cdot \tilde{K} \right) \tilde{\tau}_3(p^2, 4p^2, p^2) \equiv 3g_0 \lambda_1^{\text{lat}}. \quad (\text{B.29})
\end{aligned}$$

The tree-level corrected λ'_1 is therefore

$$\begin{aligned}\lambda'_1(p^2, 4p^2, p^2) &= \frac{\lambda_1^{\text{lat}}(p^2, 4p^2, p^2)}{\lambda_1^{(0)}(p^2, 4p^2, p^2)} \\ &= \frac{h_1(4p^2)/g_0}{3(\lambda_1^{(0)} - 4K^2\tau_3^{(0)}) - 4(4K\tilde{K} - \tilde{K}^2 - \frac{1}{2}Q^2K\tilde{K})\tilde{\tau}_3^{(0)}},\end{aligned}\tag{B.30}$$

where the p -dependence in the denominator on the last line is implicit.

C. One-loop expressions

In this section all the expressions will be given in Minkowski space. In the $\overline{\text{MS}}$ scheme, the one-loop contributions $\Sigma_1^{(1)}$, $\Pi^{(1)}$ and $\lambda_1^{(1)}$ to the quark and gluon self-energy and the vertex component λ_1 in the MOM kinematics are given by [2, 3]

$$\begin{aligned}\Sigma_1^{(1)}(p^2; \mu) &= \frac{g_{\overline{\text{MS}}}^2(\mu)}{16\pi^2} C_F \left\{ \xi \left[1 + \frac{m^2}{p^2} - \ln \frac{m^2 - p^2}{\mu^2} + \frac{m^4}{p^4} \ln \left(1 - \frac{p^2}{m^2} \right) \right] \right. \\ &\quad \left. + \frac{m^2}{p^2} \left(1 - \frac{m^2}{p^2} \right) \ln \left(1 - \frac{p^2}{m^2} \right) \right\};\end{aligned}\tag{C.1}$$

$$\begin{aligned}\Pi^{(1)}(p^2; \mu) &= \frac{g_{\overline{\text{MS}}}^2(\mu)}{16\pi^2} \left\{ \left[-\frac{97}{36} - \frac{1}{2}\xi - \frac{1}{4}\xi^2 + \left(\frac{13}{6} - \frac{\xi}{2} \right) \ln \frac{-p^2}{\mu^2} \right] C_A \right. \\ &\quad + \frac{4}{3} T_R N_f \left[\frac{1}{3} \left(5 + 12 \frac{m^2}{p^2} \right) - \ln \frac{m^2}{\mu^2} \right. \\ &\quad \left. \left. + \left(1 + \frac{2m^2}{p^2} \right) \left(1 - \frac{4m^2}{p^2} \right)^{1/2} \ln \frac{\left(1 - \frac{4m^2}{p^2} \right)^{1/2} - 1}{\left(1 - \frac{4m^2}{p^2} \right)^{1/2} + 1} \right] \right\};\end{aligned}\tag{C.2}$$

$$\begin{aligned}\lambda_1^{(1)}(p^2, 0, p^2; \mu) &= \frac{g_{\overline{\text{MS}}}^2(\mu)}{16\pi^2} \left\{ \xi C_F \left(1 + \frac{m^2}{p^2} \right) + \frac{C_A}{4} \left[(3 + \xi) + (1 - \xi) \frac{m^2}{p^2} \right] \right. \\ &\quad - \left[\xi C_F + (3 + \xi) \frac{C_A}{4} \right] \ln \frac{m^2 - p^2}{\mu^2} \\ &\quad \left. + \left[\xi C_F + (1 - \xi) \frac{C_A}{4} \right] \frac{m^4}{p^4} \ln \left(1 - \frac{p^2}{m^2} \right) \right\}.\end{aligned}\tag{C.3}$$

Setting $p^2 = -\mu^2$, this gives the following expression for the $\widetilde{\text{MOM}}$ running coupling $g_{\widetilde{\text{MOM}}}(\mu)$, in Landau gauge ($\xi = 0$) for $N_f = 0$,

$$\begin{aligned}g_{\widetilde{\text{MOM}}}(\mu) &= g_{\overline{\text{MS}}}(\mu) \left[1 + \lambda_1^{(1)}(-\mu^2, 0, -\mu^2; \mu) - \Sigma_1^{(1)}(-\mu^2; \mu) - \frac{1}{2} \Pi^{(1)}(-\mu^2; \mu) + \mathcal{O}(g^4) \right] \\ &= g_{\overline{\text{MS}}}(\mu) \left[1 + \left(\frac{151}{24} - \frac{3}{4} \frac{m^2}{\mu^2} - \frac{9}{4} \ln \left(1 + \frac{m^2}{\mu^2} \right) \right) \right. \\ &\quad \left. + \frac{m^2}{\mu^2} \ln \left(1 + \frac{\mu^2}{m^2} \right) \left[\frac{4}{3} + \frac{25}{12} \frac{m^2}{\mu^2} \right] \frac{g_{\overline{\text{MS}}}^2(\mu)}{16\pi^2} + \mathcal{O}(g^4) \right].\end{aligned}\tag{C.4}$$

In the $\overline{\text{MOM}}$ kinematics, the one-loop contributions to λ_1 and τ_3 are given by

$$\begin{aligned} \lambda_1^{(1)}(s^2, 4s^2, s^2; \mu) = & \frac{g_{\overline{\text{MS}}}^2(\mu)}{16\pi^2} \left\{ \frac{5}{4} C_A + (C_F + \frac{3}{4} C_A) \xi + \left[C_F \xi + \frac{C_A}{4} (1 - \xi) \right] \frac{m^2}{s^2} - \left[(C_F - \frac{C_A}{2}) \xi + \frac{C_A}{4} (1 + \xi) \frac{s^2 + 4m^2 s^2 + m^4}{s^2(s^2 + m^2)} \right] \ln \frac{m^2 - s^2}{\mu^2} \right. \\ & - \frac{C_A}{2} (1 + \xi) \frac{s^2}{s^2 + m^2} \ln \frac{-4s^2}{\mu^2} + \frac{C_A}{4} (1 + \xi) \frac{m^2}{s^2} \ln \frac{m^2}{\mu^2} \\ & \left. + \left[(C_F - \frac{C_A}{2}) \xi \frac{m^2}{s^2} + \frac{C_A}{4} (1 + \xi) \frac{s^2 + 4m^2 s^2 + m^4}{s^2(s^2 + m^2)} \right] \frac{m^2}{s^2} \ln \left(1 - \frac{s^2}{m^2} \right) \right\}; \quad (\text{C.5}) \end{aligned}$$

$$\begin{aligned} \tau_3^{(1)}(s^2, 4s^2, s^2; \mu) = & \frac{g_{\overline{\text{MS}}}^2(\mu)}{16\pi^2} \frac{1}{12s^2} \left\{ -(2C_F - \frac{5}{2} C_A) (2 - \xi) - \frac{C_A}{2} \xi^2 - \left[4C_F + C_A (1 - \xi) \right] \frac{m^2}{s^2} \right. \\ & - (2C_F - C_A) \left[2 + 2\xi + \frac{m^2(5 + \xi)}{s^2 - m^2} \right] \left[\sqrt{1 - \frac{m^2}{s^2}} \ln \frac{\sqrt{1 - \frac{m^2}{s^2}} + 1}{\sqrt{1 - \frac{m^2}{s^2}} - 1} + \ln \frac{m^2}{\mu^2} \right] \\ & + \left\{ 4C_F (1 + \xi) - \frac{C_A}{2} (7 - 2\xi - \xi^2) + (4C_F - C_A) \left[\frac{m^2}{s^2} \xi + \frac{3m^2}{s^2 - m^2} \right] \right. \\ & \left. - C_A \frac{m^2}{s^2 + m^2} \left[\frac{s^2}{s^2 + m^2} (5 - 4\xi - \xi^2) + \frac{m^2}{s^2} (1 + \xi) \right] \right\} \times \\ & \left. \times \left[\ln \frac{m^2 - s^2}{\mu^2} - \frac{m^2}{s^2} \ln \left(1 - \frac{s^2}{m^2} \right) \right] + \frac{C_A}{2} \frac{s^2}{(s^2 + m^2)^2} \left[s^2 (3 - 6\xi - \xi^2) + m^2 (13 - 14\xi - 3\xi^2) \right] \ln \frac{-4s^2}{\mu^2} \right\}. \quad (\text{C.6}) \end{aligned}$$

In Landau gauge, for $\text{SU}(3)$, we find in the massless limit that

$$\begin{aligned} \lambda_1'^{(1)}(s^2, 4s^2, s^2; \mu) &= \lambda_1^{(1)}(s^2, 4s^2, s^2; \mu) + 4s^2 \tau_3^{(1)}(s^2, 4s^2, s^2; \mu) \\ &= \frac{g_{\overline{\text{MS}}}^2(\mu)}{16\pi^2} \left(\frac{251}{36} + \frac{4}{9} \ln 2 - \frac{9}{4} \ln \frac{-s^2}{\mu^2} \right). \quad (\text{C.7}) \end{aligned}$$

Setting $s^2 = -\mu^2$, analogously to the $\widetilde{\text{MOM}}$ scheme, we find the $\overline{\text{MOM}}$ running coupling at asymptotically large momenta to be

$$\begin{aligned} g_{\overline{\text{MOM}}}(\mu) &= g_{\overline{\text{MS}}}(\mu) \left[1 + \lambda_1'^{(1)} - \Sigma_1^{(1)} - \frac{1}{2} \Pi^{(1)} + \mathcal{O}(g^4) \right] \\ &= g_{\overline{\text{MS}}}(\mu) \left\{ 1 + \left(\frac{4}{9} \ln 2 + \frac{793}{72} \right) \frac{g_{\overline{\text{MS}}}(\mu)}{16\pi^2} + \mathcal{O}(g^4) \right\}. \quad (\text{C.8}) \end{aligned}$$

References

- [1] W. Celmaster and R. J. Gonsalves, *The renormalization prescription dependence of the QCD coupling constant*, *Phys. Rev. D* **20** (1979) 1420.

- [2] E. Braaten and J. P. Leveille, *Minimal subtraction and momentum subtraction in QCD at two loop order*, *Phys. Rev. D* **24** (1981) 1369.
- [3] A. I. Davydychev, P. Osland and L. Saks, *Quark gluon vertex in arbitrary gauge and dimension*, *Phys. Rev. D* **63** (2001) 014022 [[hep-ph/0008171](#)].
- [4] K. G. Chetyrkin and A. Rétey, *Three-loop three-linear vertices and four-loop \widetilde{MOM} β functions in massless QCD*, [hep-ph/0007088](#).
- [5] K. G. Chetyrkin and T. Seidensticker, *Two loop QCD vertices and three loop MOM β functions*, *Phys. Lett. B* **495** (2000) 74–80 [[hep-ph/0008094](#)].
- [6] P. Weisz, *Lattice investigations of the running coupling*, *Nucl. Phys. Proc. Suppl.* **47** (1996) 71 [[hep-lat/9511017](#)];
SESAM Collaboration, A. Spitz *et. al.*, *α_s from Υ spectroscopy with dynamical Wilson fermions*, *Phys. Rev. D* **60** (1999) 074502 [[hep-lat/9906009](#)];
ALPHA Collaboration, S. Capitani, M. Lüscher, R. Sommer and H. Wittig, *Non-perturbative quark mass renormalization in quenched lattice QCD*, *Nucl. Phys. B* **544** (1999) 669–698 [[hep-lat/9810063](#)];
QCDSF-UKQCD Collaboration, S. Booth *et. al.*, *Determination of $\Lambda_{\overline{MS}}$ from quenched and $N_f = 2$ dynamical QCD*, *Phys. Lett. B* **519** (2001) 229–237 [[hep-lat/0103023](#)].
- [7] S. Bethke, *Determination of the QCD coupling α_s* , *J. Phys. G* **26** (2000) R27 [[hep-ex/0004021](#)].
- [8] A. C. Mattingly and P. M. Stevenson, *Optimization of $R_{e^+e^-}$ and ‘freezing’ of the QCD couplant at low-energies*, *Phys. Rev. D* **49** (1994) 437–450 [[hep-ph/9307266](#)].
- [9] K. Van Acoleyen and H. Verschelde, *Avoiding the Landau-pole in perturbative QCD*, [hep-ph/0203211](#).
- [10] C. D. Roberts and A. G. Williams, *Dyson-Schwinger equations and their application to hadronic physics*, *Prog. Part. Nucl. Phys.* **33** (1994) 477–575 [[hep-ph/9403224](#)].
- [11] C. D. Roberts and S. M. Schmidt, *Dyson-Schwinger equations: Density, temperature and continuum strong QCD*, *Prog. Part. Nucl. Phys.* **45S1** (2000) 1–103 [[nuc1-th/0005064](#)].
- [12] R. Alkofer and L. von Smekal, *The infrared behavior of QCD Green’s functions: Confinement, dynamical symmetry breaking, and hadrons as relativistic bound states*, *Phys. Rept.* **353** (2001) 281 [[hep-ph/0007355](#)].
- [13] **UKQCD** Collaboration, D. B. Leinweber, J. I. Skullerud, A. G. Williams and C. Parrinello, *Asymptotic scaling and infrared behavior of the gluon propagator*, *Phys. Rev. D* **60** (1999) 094507 [[hep-lat/9811027](#)].
- [14] F. D. R. Bonnet, P. O. Bowman, D. B. Leinweber and A. G. Williams, *Infrared behavior of the gluon propagator on a large volume lattice*, *Phys. Rev. D* **62** (2000) 051501 [[hep-lat/0002020](#)];
F. D. R. Bonnet, P. O. Bowman, D. B. Leinweber, A. G. Williams and J. M. Zanotti, *Infinite volume and continuum limits of the Landau-gauge gluon propagator*, *Phys. Rev. D* **64** (2001) 034501 [[hep-lat/0101013](#)].
- [15] D. Bećirević *et. al.*, *Asymptotic scaling of the gluon propagator on the lattice*, *Phys. Rev. D* **61** (2000) 114508 [[hep-ph/9910204](#)];
A. Cucchieri, *Infrared behavior of the gluon propagator in lattice Landau gauge*, *Phys. Lett. B* **422** (1998) 233–237 [[hep-lat/9709015](#)].

- [16] K. Langfeld, H. Reinhardt and J. Gattnar, *Gluon propagators and quark confinement*, *Nucl. Phys. B* **621** (2002) 131–156 [[hep-ph/0107141](#)].
- [17] L. von Smekal, A. Hauck and R. Alkofer, *A solution to coupled Dyson-Schwinger equations for gluons and ghosts in Landau gauge*, *Ann. Phys.* **267** (1998) 1 [[hep-ph/9707327](#)];
D. Atkinson and J. C. R. Bloch, *QCD in the infrared with exact angular integrations*, *Mod. Phys. Lett. A* **13** (1998) 1055 [[hep-ph/9802239](#)];
D. Zwanziger, *Non-perturbative Landau gauge and infrared critical exponents in QCD*, *Phys. Rev. D* **65** (2002) 094039 [[hep-th/0109224](#)];
C. Lerche and L. von Smekal, *On the infrared exponent for gluon and ghost propagation in Landau gauge QCD*, *Phys. Rev. D* **65** (2002) 125006 [[hep-ph/0202194](#)];
C. S. Fischer, R. Alkofer and H. Reinhardt, *The elusiveness of infrared critical exponents in Landau gauge Yang-Mills theories*, *Phys. Rev. D* **65** (2002) 094008 [[hep-ph/0202195](#)].
- [18] J. I. Skullerud and A. G. Williams, *Quark propagator in the Landau gauge*, *Phys. Rev. D* **63** (2001) 054508 [[hep-lat/0007028](#)].
- [19] J. Skullerud, D. B. Leinweber and A. G. Williams, *Nonperturbative improvement and tree-level correction of the quark propagator*, *Phys. Rev. D* **64** (2001) 074508 [[hep-lat/0102013](#)].
- [20] P. O. Bowman, U. M. Heller and A. G. Williams, *Lattice quark propagator with staggered quarks in Landau and Laplacian gauges*, *Phys. Rev. D* **66** (2002) 014505 [[hep-lat/0203001](#)].
- [21] **CSSM Lattice** Collaboration, F. D. R. Bonnet, P. O. Bowman, D. B. Leinweber, A. G. Williams and J.-B. Zhang, *Overlap quark propagator in Landau gauge*, *Phys. Rev. D* **65** (2002) 114503 [[hep-lat/0202003](#)].
- [22] F. T. Hawes, P. Maris and C. D. Roberts, *Infrared behaviour of propagators and vertices*, *Phys. Lett. B* **440** (1998) 353–358 [[nucl-th/9807056](#)].
- [23] H. Suman and K. Schilling, *First lattice study of ghost propagators in SU(2) and SU(3) gauge theories*, *Phys. Lett. B* **373** (1996) 314–318 [[hep-lat/9512003](#)].
- [24] A. Cucchieri, *Gribov copies in the minimal Landau gauge: The influence on gluon and ghost propagators*, *Nucl. Phys. B* **508** (1997) 353 [[hep-lat/9705005](#)].
- [25] R. Alkofer and L. von Smekal, *The infrared behavior of QCD propagators in Landau gauge*, *Nucl. Phys. A* **680** (2000) 133–136 [[hep-ph/0004141](#)].
- [26] J. S. Ball and T.-W. Chiu, *Analytic properties of the vertex function in gauge theories. 1*, *Phys. Rev. D* **22** (1980) 2542.
- [27] A. Kızılersü, M. Reenders and M. R. Pennington, *One loop QED vertex in any covariant gauge: Its complete analytic form*, *Phys. Rev. D* **52** (1995) 1242–1259 [[hep-ph/9503238](#)].
- [28] B. Allés *et. al.*, α_s from the nonperturbatively renormalized lattice three gluon vertex, *Nucl. Phys. B* **502** (1997) 325–342 [[hep-lat/9605033](#)];
P. Boucaud, J. P. Leroy, J. Micheli, O. Pène and C. Roiesnel, *Lattice calculation of α_s in momentum scheme*, *JHEP* **10** (1998) 017 [[hep-ph/9810322](#)];
P. Boucaud, J. P. Leroy, J. Micheli, O. Pène and C. Roiesnel, *Three-loop β function and non-perturbative α_s in asymmetric momentum scheme*, *JHEP* **12** (1998) 004 [[hep-ph/9810437](#)];
P. Boucaud *et. al.*, *Preliminary calculation of α_s from Green functions with dynamical quarks*, *JHEP* **01** (2002) 046 [[hep-ph/0107278](#)].

- [29] P. Boucaud *et. al.*, *Lattice calculation of $1/p^2$ corrections to α_s and of Λ_{QCD} in the \widetilde{MOM} scheme*, *JHEP* **04** (2000) 006 [[hep-ph/0003020](#)].
- [30] P. Boucaud *et. al.*, *Instantons and $\langle A^2 \rangle$ condensate*, *Phys. Rev. D* **66** (2002) 034504 [[hep-ph/0203119](#)].
- [31] **UKQCD** Collaboration, J. I. Skullerud, *The running coupling from the quark gluon vertex*, *Nucl. Phys. Proc. Suppl.* **63** (1998) 242 [[hep-lat/9710044](#)];
J. Skullerud, A. Kızılersü and A. G. Williams, *Quark-gluon vertex in a momentum subtraction scheme*, *Nucl. Phys. Proc. Suppl.* **106** (2002) 841–843 [[hep-lat/0109027](#)].
- [32] A. Cucchieri, *Infrared behavior of the gluon propagator in lattice Landau gauge: The three-dimensional case*, *Phys. Rev. D* **60** (1999) 034508 [[hep-lat/9902023](#)].
- [33] L. Saks, *Vertex functions in Quantum Chromodynamics*. Ph.D. thesis, University of Bergen, 2001.
- [34] S. R. Sharpe, *Improved non-perturbative renormalization without c_{NGI}* , *Nucl. Phys. Proc. Suppl.* **106** (2002) 817–819 [[hep-lat/0110021](#)].
- [35] R. Sommer, *A new way to set the energy scale in lattice gauge theories and its applications to the static force and α_s in $SU(2)$ Yang-Mills theory*, *Nucl. Phys. B* **411** (1994) 839–854 [[hep-lat/9310022](#)].
- [36] **ALPHA** Collaboration, M. Guagnelli, R. Sommer and H. Wittig, *Precision computation of a low-energy reference scale in quenched lattice QCD*, *Nucl. Phys. B* **535** (1998) 389 [[hep-lat/9806005](#)].
- [37] **UKQCD** Collaboration, K. C. Bowler *et. al.*, *Quenched QCD with $O(a)$ improvement. I: The spectrum of light hadrons*, *Phys. Rev. D* **62** (2000) 054506 [[hep-lat/9910022](#)].
- [38] C. T. H. Davies *et. al.*, *Fourier acceleration in lattice gauge theories. 1. Landau gauge fixing*, *Phys. Rev. D* **37** (1988) 1581.
- [39] P. Boucaud *et. al.*, *Testing Landau gauge OPE on the lattice with a $\langle A^2 \rangle$ condensate*, *Phys. Rev. D* **63** (2001) 114003 [[hep-ph/0101302](#)];
F. De Soto and J. Rodriguez-Quintero, *Notes on the determination of the Landau gauge OPE for the asymmetric three gluon vertex*, *Phys. Rev. D* **64** (2001) 114003 [[hep-ph/0105063](#)].
- [40] R. Alkofer, S. Ahlig and L. von Smekal, *The infrared behavior of propagators in Landau gauge QCD*, [hep-ph/9905324](#).
- [41] L. Giusti, *Lattice gauge-fixing for generic covariant gauges*, *Nucl. Phys. B* **498** (1997) 331–344 [[hep-lat/9605032](#)].
- [42] L. Giusti, M. L. Paciello, S. Petrarca and B. Taglienti, *Lattice gauge fixing for parameter dependent covariant gauges*, *Phys. Rev. D* **63** (2001) 014501 [[hep-lat/9911038](#)].
- [43] J. C. Vink and U.-J. Wiese, *Gauge fixing on the lattice without ambiguity*, *Phys. Lett. B* **289** (1992) 122–126 [[hep-lat/9206006](#)].
- [44] J. E. Hetrick and P. de Forcrand, *Smearred gauge fixing*, *Nucl. Phys. Proc. Suppl.* **63** (1998) 838 [[hep-lat/9710003](#)].
- [45] G. Heatlie, G. Martinelli, C. Pittori, G. C. Rossi and C. T. Sachrajda, *The improvement of hadronic matrix elements in lattice QCD*, *Nucl. Phys. B* **352** (1991) 266–288.
- [46] S. Capitani and G. Rossi, *Deep inelastic scattering in improved lattice QCD. 1. the first moment of structure functions*, *Nucl. Phys. B* **433** (1995) 351–389 [[hep-lat/9401014](#)].